Chapter 1 Introduction

1-1 Review of High Efficiency LEDs for Solid-State Lighting

Breakthrough in light-emitting-diode (LED) is catalyzing advances in applications of solid-state lighting (SSL).Once used only for indicator lights, LED is now replacing conventional technologies in traffic lights, exit signs, and other specialty application [1.1]. The main applications and their corresponding luminous efficiency of LED in recent years are predicted in Fig. 1.1. In this figure, the productions adopting LED technology are enormous and the demanding for high luminous efficiency LED is intense. For SSL consideration, the luminous efficiency of LED shall be larger than that of fluorescent lamps, 80lm/W, at least. Although the applications of LED are diverse and significant, the ultimate achievement of LED is to completely replace conventional lighting (filament and fluorescent lamps) and realize SSL in the future [1.2]. According to U.S. department of energy (DOE) [1.3], buildings consume 71 % of the total electricity used in the U.S. today. Lighting alone accounts for 30 % of the electricity consumption in buildings, as shown in Fig. 1.2. Assuming reasonable growth rate, by the year 2025 the U.S. may be using as much as 1,000 Terawatt-hour (TWh) of electricity for lighting. Worldwide, the energy used for lighting is estimated to be three to four times greater [1.4]. If 50 % efficient SSL were to be achieved and displaced current white-lighting technologies completely, the electricity used for lighting would be cut by 62 %, as shown in Fig. 1.3. Fig.1.3 shows the transformations of LED applications within several decades. The LED lighting began in the 2000s, and will be mainly focus on the LCD backlight application for the next decade. After two decades later, the LED is expected to be popularly used for SSL. In addition, the saving in energy production that could be enabled by SSL would also have an important impact on the environment. The energy saved through SSL

would reduce carbon emission to the atmosphere as well. Therefore, the LED plays a significant role as for the considerations of energy conservation and environment protection.

It is also important to review the development history of LED since it has so many profound and enormous influences over our living environment as mentioned above. The LEDs, providing the direct conversion of energy to light via the manipulation of electrons in a solid at room temperature, started to develop in the 1960s. The GaAsP/GaAs was the first material system applied for red color LEDs. However, due to the lattice mismatched between GaAsP and GaAs, a bunch of dislocation defects appears in GaAsP epitaxial film. As compared to conventional incandescent or fluorescent lamp, an extraordinary low luminous efficiency (~ 0.1 lm/W) was obtained on this prototype LED device. After around 50-year sustained development, the luminous efficiency of LEDs has exceeded conventional lighting source, opening up the window of solid-state-lighting. The historical development of the luminous efficiency of visible-spectrum LEDs and their corresponding epitaxial materials is shown in Fig. 1.4 [1.5]. According to Fig. 1.4, the state-of-the-art visible-spectrum LEDs are dominated by two material systems, $(Al_xGa_{1-x})_{1-y}In_yP$ and $In_xGa_{1-x}N$. The $(Al_xGa_{1-x})_{1-y}In_yP$ material system was developed in the late 1980s and become the fundamental material system used for high brightness LEDs emitting in the red, orange, amber, and yellow wavelength regions. The electronic energy bandgap versus lattice constant of $(Al_xGa_{1-x})_{1-y}In_yP$ material system is shown in Fig. 1.5 [1.6]. The $(Al_xGa_{1-x})_{1-y}In_yP$ is lattice matched to GaAs for $y = 0.48$ and direct bandgap emission is available from $x = 0$ (~650-nm, deep red) to $x = 0.53$ (~560-nm, yellow-green). Besides, due to the intense researches over the last 15 years [1.7-1.16], high material quality of AlGaInP LEDs have been demonstrated and massively produced by metal-organic chemical vapor deposition (MOCVD).

Fig. 1.5 also depicts the energy bandgap for the wurtzite III-nitride material system. The $In_xGa_{1-x}N$ material system was developed in the early 1990s and become the primary material system for commercially available LEDs emitting from ultraviolet (~365-nm) to deep green (~550-nm) in the late 1990s. Unlike $(Al_xGa_{1-x})_{1-y}In_yP$ material system, the epitaxial quality of $In_xGa_{1-x}N$ material system is relative poor due to the absence of suitable basal substrate. Today's $In_xGa_{1-x}N$ LEDs are usually grown on either sapphire ($a \sim 2.75$ Å) or silicon carbide ($a \sim 3.08$ Å) substrates. $In_xGa_{1-x}N$ material grown on these lattice-mismatch substrates usually suffers from high density of dislocation defects (10^8-10^{10} cm^{-2}). Carriers can leak through these dislocation defects and recombine non-radiatively, thereby compromising device performance. Moreover, the wurtzite crystal structure provides for spontaneous and piezoelectric polarization within the InGaN layer that causes large built-in electric fields along the c-axis [1.17-1.18], complicating device operation and characterization of basic optical process. Therefore, more comprehensive considerations shall be taken while designing the high brightness InGaN-based blue or green LEDs. Although the fundamental issues of InGaN-based LEDs is relative complicated than that of AlGaInP-based LEDs, the efficiency improvement of blue and green LEDs is extremely expeditious due to the intense researches on this material system in recent years [1.19-1.26], as also shown in Fig. 1.4. The state-of-the-art performance of high power LEDs versus emission wavelength was shown in Fig. 1.6. This figure reflects the characteristics of the III-V material systems as mentioned above. Although AlGaInP-based LEDs have superior epitaxial quality, the overall performance, external quantum efficiency, is compromised with the small escape cone of emitting photons (the refractive index ~ 3.5 for AlGaInP) and strong material absorption. For InGaN-based LEDs, even they have relatively poor epitaxial quality; reasonably high internal quantum efficiencies

3

are still obtained, especially for relatively low InN mole fractions due to the formation of In-rich clusters or quantum dots during the growth of InGaN multiple quantum wells. Besides, the difference of refractive index between InGaN material and surrounding materials is smaller than that of AlGaInP material system (the refractive index ~ 2.4 for InGaN); larger escape cone of emitting photons is expected for InGaN-based LEDs. Therefore in Fig. 1.6, a little higher external quantum efficiency was observed for InGaN-based LEDs (~ 58 %, at 400-nm), as compared to that of AlGaInP-based LEDs (~ 55 %, at 650-nm). However, as considering the applications of solid-state lighting, the performance of the state-of-the-art LEDs discussed above is still low and needed to be further enhanced. In addition, for lighting application we have to take package-loss and phosphor converting issues into account. Therefore, the purpose of this thesis is to boost external quantum efficiency of visible-spectrum LEDs by resolving the fundamental restrictions limiting LEDs performances. For AlGaInP-based LEDs, it is easily to achieve 90 % internal quantum efficiency, even as high as the value of 99 % is feasible for an extraordinarily good crystalline quality. Thus the primary issue for AlGaInP-based LEDs is to enhance light extraction efficiency restricted by the Snell's law. For InGaN-based LEDs, we propose a novel lateral overgrowth technology adopting chemical wet etching-patterned sapphire substrate (CWE-PSS). The aim of this proposed structure is to reduce threading dislocation defects by lateral overgrowth occurred on CWE-PSS and increase the escape probability of trapped photons via optical diffraction by CWE-PSS; therefore, both internal quantum and light extraction efficiencies can be enhanced simultaneously based on this novel structure. For white light emission, in order to reduce phosphor converting issue commonly observed on commercial available white light LEDs, we propose a phosphor-free complementary dual-wavelength LED (470-nm/550-nm) by using sapphire laser-lift-off (LLO) and wafer-bonding schemes.

The luminous efficiency of this novel LED structure can achieve to around 120lm/W,

and has great potential to facilitate the early coming of SSL.

1-2 Organization of the Thesis

This thesis is divided into five chapters. First chapter is a brief review of high efficiency visible-spectrum LEDs for solid-state lighting applications, as mentioned in section 1-1.

In Chapter 2, we briefly introduce the fundamental of LED science and several important criteria or physical parameters used to define and judge LED performances. The main challenges for achieving high efficiency AlGaInP- and InGaN-based LEDs are also discussed, including the fundamental of materials systems, geometrical shape of LED designs, and LED packages issues.

In Chapter 3, we investigate the mechanism responding for performance enhancement of InGaN-based LEDs grown on chemical wet etching-patterned sapphire substrate (CWE-PSS) with V-Shaped pit features on the top surface. The V-shaped pits roughening surface is investigated by using scanning electron microscope (SEM) and transmission electron microscopy (TEM) and a paraboloidal autocorrelation function theoretically modeling the V-shaped pits roughening surface is also given , demonstrating this roughening surface performs as a strong diffuser. To quantitatively verify the efficiency improvement of our proposed LED structure benefiting from, three different LED structures are fabricated and compared with each other. We use TEM and temperature dependent photoluminescence (PL) to investigate the threading dislocations and estimate internal quantum efficiency of the sample grown on CWE-PSS. We also measure the optical diffraction by CWE-PSS to study its efficiency as a trapped light extractor. The results suggest that the observed enhancement in internal quantum efficiency and light extraction efficiency can be accounted for by the reduction in threading dislocations in active region and optical diffraction of trapped light by the CWE-PSS, respectively.

In Chapter 4, by combining sapphire laser lift-off and wafer-bonding schemes, we

fabricate InGaN-based phosphor-free dual-wavelength blue/green (470-nm/550-nm) LEDs with three terminal operations. The novel concept can provide a monolithic and dichromatic white lighting source, and most important, eliminate the low phosphor converting issue usually occurred in conventional white light LEDs. The device is equivalent to a parallel connection of blue and green LEDs, thus effective electrical resistance of the device could be reduced. The maximum luminous efficiency is around 120lm/W, accompanying with a broad electroluminescence emitting with combination of blue and green colors. Therefore, this integrated dichromatic lighting structure has great potential to facilitate the early coming of solid-state-lighting.
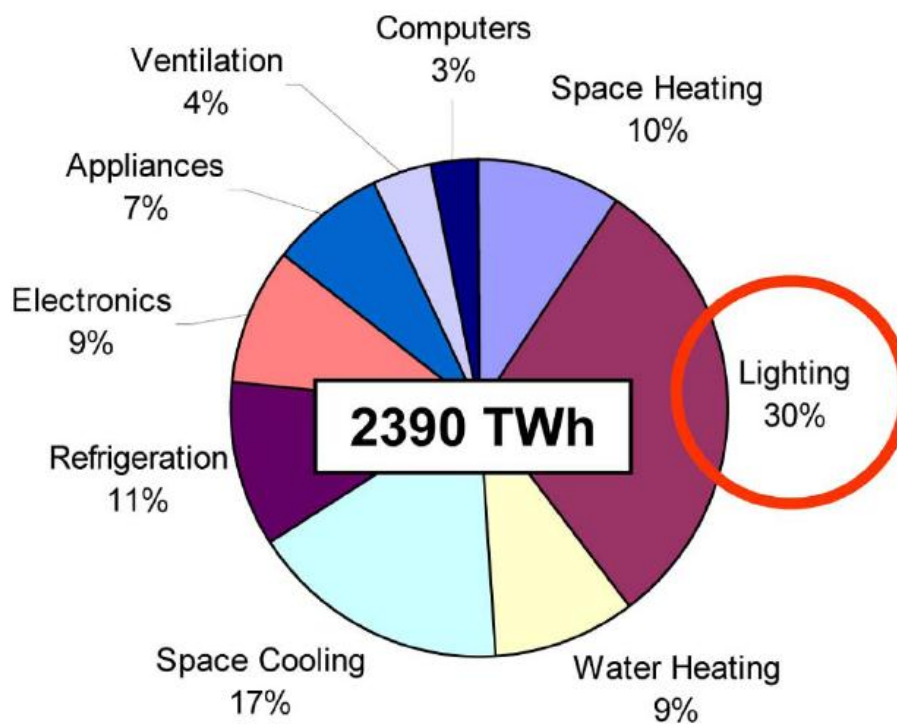
Finally, conclusions of this thesis and suggestions for future works are included in Chapter 5.
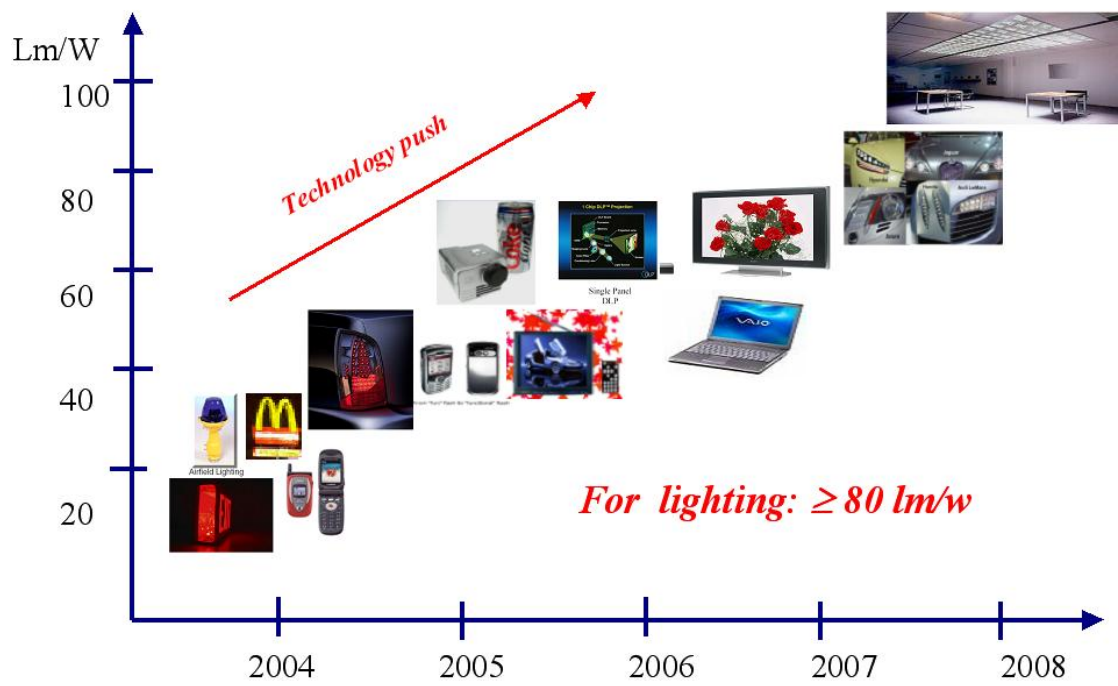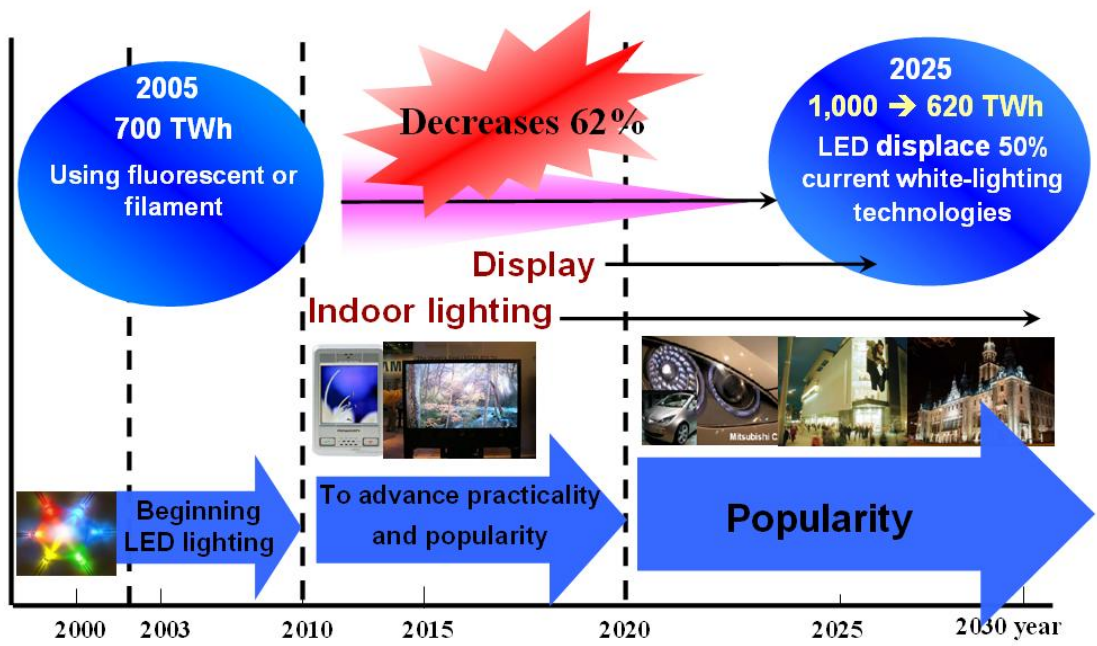
Fig. 1.1 Roadmap of LED application in lighting (quoted from Epistar Corporation).
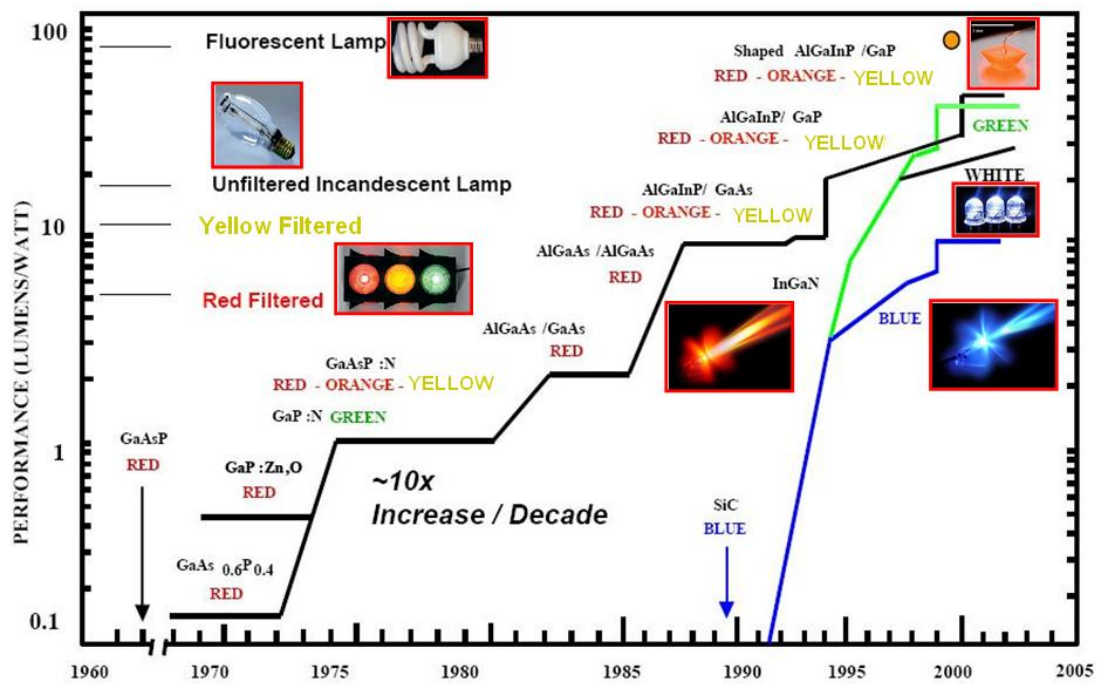
Fig. 1.2 Lighting accounts for 30 % of the electricity consumed by U.S. buildings (quoted from James Brodrick [1.3]).
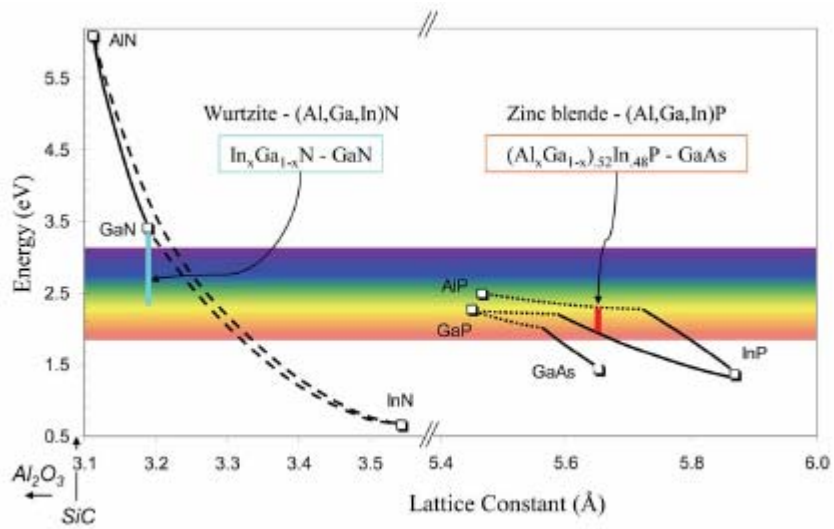
**Fig. 1.3** Lighting accounts for 30 % of the electricity consumed by U.S. buildings (quoted from James Brodrick [1.3]).

Fig. 1.4 Evolution of luminous efficiency of visible-spectrum LEDs and their corresponding epitaxial materials (quoted from Craford [1.5]).

Fig. 1.5 Energy Bandgap versus lattice constant for wurtzite III-nitride and zinc-blende III-phosphide semiconductor alloy systems (quoted from Krames [1.6]).
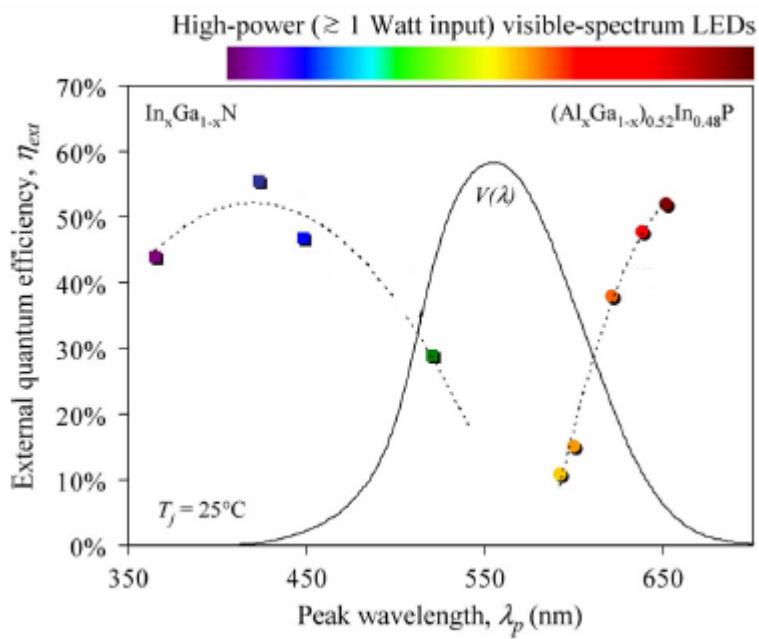
Fig. 1.6 State of the art external quantum efficiency for high-power visible-spectrum LEDs (quoted from Philips Lumileds Corporation).

References of Chapter 1

[1.1] E. F. Schubert, *Light-emitting diodes,* (Second Edition, Cambridge University Press, Cambridge, U.K., 2006.)

[1.2] M. G. Craford, N. Holonyak, Jr., and F. A. Kish, Jr., "In pursuit of the ultimate lamp," *Scientific Amer.*, pp. 83–88, Feb. 2001.

[1.3] James Brodrick, "Next-Generation Lighting Initiative at the U.S. Department of Energy: Catalyzing Science into the Marketplace," IEEE Journal of Display Technology, pp. 91-97 (2007).

[1.4] "Basic Research Needs for Solid-State Lighting," report of the basic energy sciences workshop on solid-state lighting, Maryland May (2006).

[1.5] Craford M. G. "The brightness future of light-emitting diodes," Plenary talk on light emitting diodes at the MRS Fall Meeting, Boston Massachusetts December (1999).

[1.6] Michael R. Krames et al, "Status and Future of High- Power Light-Emitting Diodes for Solid-State Lighting," IEEE Journal of Display Technology, pp. 160-175 (2007).

[1.7] H. Sugawara, M. Ishikawa, and G. Hatakoshi, "High-efficiency In- GaAlP/GaAs visible light-emitting diodes," Appl. Phys. Lett., vol. 58, pp. 1010–1012, 1991.

[1.8] K. H. Huang et al., "Twofold efficiency improvement in high performance AlGaInP light-emitting diodes in the 555–620 nm spectral region using a thick GaP window layer," Appl. Phys. Lett., vol. 61, pp. 1045–1047, 1992.

[1.9] F. A. Kish et al., "Very high-efficiency semiconductor wafer-bonded transparent-substrate $(Al_xGa_{1-x})_{0.5}In_{0.5}$P/GaP light-emitting diodes," Appl. Phys. Lett., vol. 64, pp. 2839–2841, 1994.

[1.10] M. R. Krames et al., "High-power truncated-inverted-pyramid $(Al_xGa_{1-x})_{0.5}In_{0.5}$

P/GaP light-emitting diodes exhibiting >50% external quantum efficiency," Appl. Phys. Lett., vol. 75, pp. 2365–2367, 1999.

[1.11] Th. Gessmann and E. F. Schubert, "High-efficiency AlGaInP light-emitting diodes for solid-state lighting applications," Journal of Appl. Phys., vol. 95, pp. 2203-2216, 2004.

[1.12] Y. J. Lee, H. C. Kuo, S. C. Wang, T. C. Hsu, M. H. Hsieh, M. J. Jou, and B. J. Lee "Increasing the extraction efficiency of AlGaInP LEDs via n-side surface roughening", IEEE Photonic Technology Letter, Vol. 17, No. 11, pp2289-2291, NOVEMBER, 2005.

[1.13] Y. J. Lee, H. C. Tseng, H. C. Kuo, S. C. Wang, C. W. Chang, T. C. Hsu, Y. L. Yang, M. H. Hsieh, M. J. Jou, and B. J. Lee, "Improvement in Light-Output Efficiency of AlGaInP LEDs Fabricated on Stripe Patterned Epitaxy", IEEE Photonic Technology Letter, Vol. 17, No. 12, pp2532-2534, DECEMBER, 2005.

[1.14] Y. J. Lee, T.C. Lu, H.C. Kuo, S.C. Wang, M. J. Liou, C.W. Chang, T. C. Hsu, M. H. Hsieh, M. J. Jou, and B. J. Lee, "AlGaInP LEDs with Stripe Patterned Omni-Directional Reflector", Japanese Journal of Applied Physics, Vol. 45, Part 1, No. 2A, pp643-645, Feb. 2006.

[1.15] Y. J. Lee, T.C. Lu, H.C. Kuo, S.C. Wang, M. J. Liou, C.W. Chang, T. C. Hsu, M. H. Hsieh, M. J. Jou, and B. J. Lee, "High brightness AlGaInP-based light emitting diodes by adopting the stripe-patterned omni-directional reflector", Semicond. Sci. Technol. Vol.21, pp.184–189, 2006.

[1.16] Y. J. Lee, H. C. Kuo, S. C. Wang, T. C. Hsu, M. H. Hsieh, M. J. Jou, and B. J.Lee "Nano-roughening n-side surface of AlGaInP-based LEDs for increasing extraction efficiency", Material Science and Engineering: B, accept for publication.

[1.17] F. Bernardini, V. Fiorentini, and D. Vanderbilt, "Spontaneous polarization and piezoelectric constants of III-V nitrides," Phys. Rev. B, vol. 56, pp. R10024–R10027,

1997.

[1.18] T. Takeuchi et al., "Determination of piezoelectric fields in strained GaInN quantum wells using the quantum-confined Stark effect," Appl. Phys. Lett., vol. 73, pp. 1691–1693, 1998.

[1.19] S. Nakamura, M. Senoh, and T. Mukai, "High-power InGaN/GaN double-heterostructure violet light emitting diodes," Appl. Phys. Lett., vol. 62, pp. 2390–2392, 1993.

[1.20] S. Nakamura, M. Senoh, N. Iwasa, and S.-I. Nagahama, "High-power InGaN single-quantum-well-structure blue and violet light-emitting diodes," Appl. Phys. Lett., vol. 67, pp. 1868–1870, 1995.

[1.21] S. Nakamura, M. Senoh, S. Nagahama, N. Iwasa, T. Yamada, T. Matsushita, H. Kiyoku, and Y. Sugimoto, "InGaN-based multi-quantumwell- structure laser diodes," Jpn. J. Appl. Phys., vol. 35, pp. L74–L76, 1996.

[1.22] S. J. Rosner, E. C. Carr, M. J. Ludowise, G. Girolami, and H. I. Erikson, "Correlation of cathodoluminescence inhomogeneity with microstructural defects in epitaxial GaN grown by metalorganic chemical-vapor deposition," Appl. Phys. Lett., vol. 70, pp. 420–422, 1997.

[1.23] S. Nakamura, "The roles of structural imperfections in InGaN-based blue light-emitting diodes and laser diodes," Science, vol. 14, pp. 956–961, 1998.

[1.24] Y. J. Lee, J.M.Hwang, T. C. Hsu, M. H. Hsieh, M. J. Jou, B. J. Lee, T.C. Lu, H.C. Kuo, and S.C. Wang, "GaN-based LEDs with Al-Deposited V-Shape Sapphire Facet Mirror," IEEE Photonic Technology Letter, Vol. 18, No. 8, pp.724-726, March, 2006.

[1.25] Y. J. Lee, J.M.Hwang, T. C. Hsu, M. H. Hsieh, M. J. Jou, B. J. Lee, T.C. Lu, H.C. Kuo, and S.C. Wang, "Enhancing Output Power of GaN-based LEDs Grown on Chemical Wet Etching Patterned Sapphire Substrate," IEEE Photonic Technology

Letter, Vol. 18, pp.1152-1154, 2006.

[1.26] Y. J. Lee, H.C. Kuo, T.C. Lu, H.C. Kuo, B.J.Su, and S.C. Wang, "Fabrication and characterization of GaN-based LEDs grown on Chemical Wet Etching Patterned Sapphire Substrate," Journal of The Electrochemical Society, 153 (12) G1106-G1111,2006.

Chapter 2 LED science overview and research challenges

2-1 Background

2-1-1 Introduction for LEDs Operations

LEDs are designed semiconductor structures within which electrical energy is converted to light through a complex sequence of steps. At each step in the sequence, energy can be lost. As illustrated in Fig. 2.1., the major stages of LED operation are as follows:

1. Injection and transport of negatively charged electrons and positively charged holes;

2. Electron and hole radiatively recombine to form a photon within the LED chip;

3. Extraction of photons from the LED chip into the surrounding materials;

4. Mixing of these photons with similarly produced photons of other colors (e.g., Red, Green and Blue LEDs), or conversion of these photons into photons with longer wavelengths (e.g., Blue LED with yellow phosphors).

The first step is injection of electrons and holes into the negatively doped (n-type) and positively doped (p-type) contact layers of the LED, respectively. The injection takes place through metallic contacts, typically of different materials with electronic characteristics specifically used for n-type and p-type. Typically, the injection is not 100% efficient because contact resistance leads to resistive losses in the process of injecting charge from the metallic contact into the semiconductor. In addition, the lateral spread of these electrons and holes to access all portions of the LED's active layer is also an important issue in this operation stage [2.1]. These semiconductor current-spreading layers also need to have very low resistance so that resistive losses

do not decrease a portion of the input energy. In this stage, an improved understanding of doping, and especially p-doping, in wide-bandgap semiconductors represents a major research challenge.

The next stage of LED operations is the birth of the photon. Electrons and holes move into the active layer, typically a series of quantum wells, layers of lower-bandgap semiconductors into which electrons and holes are attracted. Electrons and holes then annihilate each other, with their net energy being given up as a photon or light particle. This process is referred to as radiative recombination. On the other hand, another type of electron-hole recombination exists: nonradiative recombination [2.2-2.3]. In this case, the electron and hole also annihilate each other, but instead of producing a photon, they produce unwanted heat, in the form of vibrations of the lattice of atoms in the crystal. This energy is wasted and reduces the overall efficiency of the LED. The possible recombinative paths of injected electrons and holes are shown in Fig. 2.2. Typically, material defects —including defects that extend over some distance of the material such as threading dislocations and more localized point defects such as vacancies and impurities — act as centers of nonradiative recombination. Thus the overall goal in this stage is to enhance the radiative recombination rate and suppress the nonradiative recombination rate.

Once a photon has been born in the active layer of the LED, it is still a long way from being useful for illumination. The next stage in LEDs operations is its extraction from the LEDs. This extraction is relatively inefficient. Typically, only a fraction of the photons produced within the LED active layer escape from the semiconductor crystal into the surrounding air. Light generated inside a semiconductor cannot escape from the semiconductor if it is totally internally reflected at the semiconductor-air interface. If the angle of incidence of a light ray is close to normal incidence, light can escape from the semiconductor. However, total internal reflection occurs for light rays

with oblique incidence. Total internal reflection severely reduces the external efficiency, in particular for LEDs consisting of high-refractive-index materials. The calculation of light escape cone has been report by Schubert [2.4].

Assume that the angle of incidence in the semiconductor at the semiconductor- air interface is given by θ_1. Then the angle of incidence of the refracted ray, θ_2, can be derived from Snell's law

$$n_s \, sin\theta_1 = n_a \, sin\theta_2 \tag{2-1}$$

where n_s and n_a are the refractive indices of the semiconductor and air, respectively. The critical angle for total internal reflection is obtained using $\theta_2 = 90°$, using Snell's law, one obtains

$$sin\theta_c = (n_a/n_s) \, sin \, 90° = n_a/n_s \quad ; \quad \theta_c = sin^{-1} \, (n_a/n_s) \tag{2-2}$$

.

The angle of total internal reflection defines the light-escape cone. Light emitted into the cone can escape from the semiconductor, whereas light emitted outside the cone is suffered from the total internal reflection.

The surface area of the escape cone is given by the integral

$$Area = \int dA = \int_{\theta=0}^{\theta_c} 2\pi r \sin\theta r d\theta = 2\pi r^2 (1 - \cos\theta_c) \tag{2-3}$$

Assume that light is emitted from a point-like source in the semiconductor with a total power of P_{source}. Then the power that can escape from the semiconductor is given by

$$P_{escape} = P_{source} \frac{2\pi r^2 (1 - \cos\theta_c)}{4\pi r^2} \tag{2-4}$$

where $4\pi r^2$ is the entire surface area of the sphere with radius r.

The calculation indicates that only a fraction of the light emitted inside a semiconductor can escape from the semiconductor. This fraction is given by

$$\frac{P_{escape}}{P_{source}} = \frac{1}{2}(1 - \cos\theta_c)$$
(2-5)

Expanding Eq (2-5) into power series and neglecting higher than second-order terms yields

$$\frac{P_{escape}}{P_{source}} = \frac{1}{2}\left[1 - \left(1 - \frac{\theta_c^2}{2}\right)\right] = \frac{1}{4}\theta_c^2 \approx \frac{1}{4}\frac{n_a^2}{n_s^2}$$
(2-6)

According to Eq (2-6), only a few percent of the light generated in the semiconductor can escape from a planar LED.

Figure 2.3 shows an example of extraction efficiency of a conventional InGaN-based LED calculated by above equations, only 12% light emitting from active regions can be extracted outside LED chips, most light, ~66%, are trapped inside LED chips. Indeed, these trapped photons bounce around within the crystal until they are eventually absorbed by a crystal defect, a surface state, or metal contact surfaces. Thus in this stage of LEDs operations, exploring novel approaches to photon manipulation and extraction, and improving our understanding of the physics of photon-matter interaction are major research challenges.

Even though a photon has been extracted from the LED crystal, it may not be at a wavelength optimal for illumination purposes. For general illumination, it is necessary to produce white light, i.e., light composed of a mixture of photons that appears white to the human eye and that accurately renders the colors of objects. The final stage in

LEDs operations involves converting the wavelengths of photons into those suitable for such white light. The most applied approach to produce white light LED, illustrated on Fig.2.4, is to use photon conversion materials, including phosphors or semiconductors. These materials absorb some or all of the photons directly emitted from the LED and then re-emit new photons at longer wavelengths. In this way, for instance, a blue LED can be converted to a white LED by coating its surface with yellow phosphors. A portion of the blue light is transmitted, while the rest is absorbed by the phosphor and reemitted as yellow. Mixed together, the light appears white.

This is the dominant approach used with most commercially available white LEDs now. Currently, photon conversion materials suffer from insufficient efficiencies on the order of 70% to 80%. Efficiencies are even lower for phosphors that emit in the red, but red is a necessary component of white lighting that accurately renders the colors of real-world objects. Thus in this stage of LEDs operations, exploring new materials and approaches for photon conversion are major research challenges.

At each stage in LEDs operations mentioned above, inefficiencies and parasitic processes cause energy to be lost, so the final amount of energy in the form of photons illuminating is a small fraction of the initial energy. Therefore, the main purpose of this thesis is to improve processes and avoid loss of input energy at each stage as discussed above by sophistically associating with the design, synthesis, and characterization of the materials and structures that comprise LEDs.

2-1-2 Definition of Physical Parameters Related to LEDs

In this section, we briefly introduce and derive several important physical parameters, including internal, extraction, external, and power efficiencies, which were widely used to analyze LEDs performances. Starting from rate equation and discussing system under steady-state, i.e., the carrier generation rate equating to the carrier recombination rate, to derive the dependence of internal quantum efficiency with radiative and nonradiative recombination rates. Then, others efficiencies (extraction, external, and power efficiencies) related to LEDs can be derived sequentially.

For the double heterostructure active region, the injected current provides a generation term and various radiative and nonradiative recombination processes as well as carrier leakage provides recombination term. The process of a certain steady-state carrier density in the active region could be compared to that a reservoir analogy, which is being simultaneously filled and drained, as shown in Fig. 2.5. In Fig.2.5, there are $\eta_i(I/eV)$ electrons per second per unit volume being injected into the active region. The η_i, is the fraction of terminal current that generates carriers in the active region and V is the volume of the active region.

Thus, rate equation is determined as

$$\frac{dn}{dt} = G_{gen} - R_{rec} \qquad (2\text{-}7)$$

where G_{gen} is the rate of injected electrons and R_{rec} is the rate of recombining electrons per unit volume in the active region.

The recombination process is accompanied with spontaneous emission rate, R_{sp}, nonradiative recombination rate, R_{nr}, and carrier leakage rate, R_l, as depicted in Fig.

2.5. Carrier leakage rate, R_l, is occurred when the transverse or lateral potential barriers are not sufficiently high. Thus total recombination rate is expressed as below

$$R_{rec} = R_{sp} + R_{nr} + R_l \qquad (2\text{-}8)$$

It is common to describe the natural decay processes by a carrier lifetime, τ. In the absence of photon generation term, the rate equation for carrier decay is,

$$dn/dt = n/\tau\,, \qquad (2\text{-}9)$$

where $n/\tau = R_{sp} + R_{nr} + R_l$,

.The carrier rate equation in equivalent be expressed as

$$\frac{dn}{dt} = \frac{\eta_i I}{eV} - \frac{n}{\tau} \qquad (2\text{-}10)$$

The spontaneous photon generation rate per unit volume is exactly equal to the spontaneous electron recombination rate, R_{sp}, since by definition every time an electron-hole pair recombines radiatively, a photon is generated. Under steady-state conditions ($dn/dt = 0$), the generation rate equals the recombination rate, i.e.,

$$\frac{\eta_i I}{eV} = \frac{n}{\tau} = R_{sp} + R_{nr} + R_l \qquad (2\text{-}11)$$

The spontaneously generated optical power, P_{sp}, is obtained by multiplying the number of photons generated per unit time per unit volume, R_{sp}, by the energy per photon, hv, and the volume of the active region, V.

Then

$$P_{sp} = h\nu V R_{sp} = \eta_i \eta_r \frac{h\nu}{e} I \qquad (2\text{-}12)$$

where the radiative efficiency, η_r, is defined as

$$\eta_r = \frac{R_{sp}}{R_{sp} + R_{nr} + R_l} \qquad (2\text{-}13)$$

Usually, the η_r depends upon the carrier density and the product of $\eta_i\eta_r$ is the internal quantum efficiency, η_{int}. Thus according to Eq (2-12), the internal quantum efficiency is defined as:

$$\eta_{int} = \frac{P_{sp}/(h\nu)}{I/e} = \eta_i \eta_r \qquad (2\text{-}14)$$

= (the number of photons emitted from active region per secend)/(the number of electrons injected into LED per secend)

Thus the internal quantum efficiency is related to η_i, the fraction of terminal current that generates carriers in the active region, and to η_r, the fraction of rates between radiative recombination to total carriers' recombination. According to Eq (2-14), we can enhance the internal quantum efficiency of LEDs by either increasing radiative recombination rate, R_{sp}, or decreasing nonradiative recombination rate, R_{nr}, and carrier leakage rate, R_l. Therefore, significantly improvements of grown-layers quality associating with appropriate design of LEDs structures is the main thought to improve the internal quantum efficiency.

In an ideal LED, all photons emitted by the active region can be emitted into free

space. Such an LED has unity light extraction efficiency. However, in a real case, not all the power emitted from the active region is emitted into free space. This is due to several possible loss mechanisms, such as re-absorption of the LED substrate, reflection by the contact metallic surfaces, and most commonly, the total internal reflection at semiconductor/air interface.

The light extraction efficiency is defined as

$$\eta_{extraction} = \frac{p/(h\nu)}{P_{sp}/(h\nu)} \tag{2-15}$$

= (the number of photons emitted into free space per second)/ (the number of photons emitted from active region per second)

Where p is the optical power emitted into free space.

For the conventional LEDs, the extraction efficiency is relative small due to the large difference of refractive index between semiconductor materials and surrounding matrix (encapsulated epoxy or sir). The light extraction efficiency for most LED structures is less than 50% and significantly depends on emitting wavelengths and chip sizes. There is typically a trade-off in chip design: larger chips produce more light, but allow less of the light to escape. On the other hand, smaller chips will have higher overall efficiency, but will emit less light. The light extraction efficiency of conventional InGaN-based LEDs is larger than that of conventional AlGaInP-based LEDs due to the absence of absorbed substrates. Since the light extraction efficiency of LEDs structure is relative small, many previous researches had put enormous efforts to enhance this value. The relative research techniques include chip shaping, surface texturing, photonic crystals, and resonant cavity LEDs. Above techniques often involve with several highly sophisticated and costly device processes [2.5-2.6].

The external quantum efficiency is defined as

$$\eta_{ext} = \frac{P/(h\nu)}{I/e} \quad = \quad \eta_{int}\eta_{extraction} \tag{2-16}$$

= (the number of photons emitted into free space per second)/ (the number of electrons injected into LED per second)

The external quantum efficiency gives the ratio of the number of useful light particles to the number of injected charge particles. According to Eq (2-16), the numbers of photons emitted outside LED chips to free space is dominated by two efficiencies: internal quantum efficiency and extraction quantum efficiency. In order to boosting the LEDs output power, we can enhance either internal quantum efficiency or light extraction efficiency; the best circumstance, or we can design a novel LED structure that can enhance them both. For past decades, many researches had paid attention towards to this goal. Typically these researches can be divided into two categories based on the epitaxial materials: AlGaInP- or InGaN-based LEDs. For AlGaInP-based LED grown on the lattice-match GaAs substrate, extremely high internal quantum efficiency could be achieved without a doubt, thus main studies were focus on the enhancement of the light extraction efficiency. On the other hand, many efforts had paid to enhance both the internal quantum efficiency and light extraction efficiency of InGaN-based LED due to its absence of lattice-match epitaxial substrate. The general idea of attaining high internal efficiency is increasing the radiative recombination probability or decreasing that of the non-radiative recombination by improving epitaxail quality. As for the consideration of light extraction efficiency, sophistical LED chip designs eliminating the optical loss by

substrate, metallic ohmic contact surfaces and total internal reflection are necessary.

The power efficiency is defined as

$$\eta_{power} = \frac{P}{IV} \qquad\qquad (2\text{-}17)$$

Where IV is the electrical power provided to the LED. Informally, the power efficiency is also called the wallplug efficiency. This value is commonly used to assert the LED performance since it is relative easier to measure in real LED as compared to other physical parameters of LED discussed above.

2-2 Main Challenges for High Efficiency LEDs

2-2-1 Quality of Epitaxial Material

AlGaInP Materials

The $(Al_x,Ga_{1-x})_{1-y}In_yP$ alloys are nearly lattice matched to GaAs, and production of LEDs emitting from 555 nm (yellow-green) to 650 nm (deep red) is a relatively mature technology. The availability of single crystal GaAs substrates enables growth of high-quality phosphide material by MOCVD. For low Al fraction, the internal quantum efficiency approaches 100%. $(Al_xGa_{1-x})0.5In0.5P$ is a direct bandgap semiconductor for $x < 0.5$; above that composition, it is an indirect-gap material. The crossover occurs at bandgap energy of about 2.23 eV (555 nm). Thus, the AlGaInP LED quantum efficiency drops precipitously at shorter wavelengths because of the approach of the direct-indirect bandgap crossover. That is, as the indirect-gap X-band becomes more populated, the radiative lifetime increases, allowing other nonradiative processes to become more dominant. However, owing to the low energy bandgap of GaAs is 1.42 eV (870 nm) at room temperature, so this substrate absorbs emitted light below this wavelength, greatly lowering the efficiency of AlGaInP-based LEDs. Figure 2.6 shows two common approaches applied on industrial lines to prevent absorption of emitted light by the substrate. One is to insert a Distributed Bragg Reflector (DBR) between the LED active region and substrate. However, only the radiated light impinging near normal to the DBR can be effectively reflected. As for the oblique angles of radiated light, the DBR becomes transparent and the light is subsequently absorbed by the GaAs substrate. A more significant improvement of the extraction efficiency can be achieved by replaced the GaAs absorbing substrate by a GaP transparent substrate (TS) through a wafer bonding process. However, the process is costly and complicated. Recently, an omni-directional reflector (ODR) was proposed and applied on AlGaInP-based LEDs, which provides a comparable

approach to improve the light extraction efficiency compared to the GaP TS LEDs. It also offers a cost advantage over TS technique and superior enhanced efficiency over DBR technique.

InGaN Materials

For $In_xGa_{1-x}N$ alloys, the major difficulty is the lack of low-cost, single-crystal GaN to use as a growth substrate. Gallium nitride (GaN) is now widely studied by growing it heteroepitaxially on other hexagonal substrates, usually sapphire or silicon carbide (SiC). These substrates must be used because wafers of GaN are not available as in the case of more common semiconductors. A layer grown at lower temperature, the nucleation layer, is used to initiate oriented growth on the substrate, followed by epitaxial growth on this layer at higher temperatures. However, there is a serious mismatch in the distance of atomic spacing of GaN with respect to those of sapphire (lattice mismatch +16%, thermal expansion mismatch +39%) and more expensive silicon carbide (lattice mismatch -3.5%, thermal expansion mismatch -3.2%). Growth of GaN on planar sapphire substrates results in high densities of (10^8 -10^{10} /cm^2) dislocation defects, resulting in defect-mediated nonradiative recombination of electron-hole pairs and reduced mobility because of carrier scattering from charged defect centers. These dislocations defects thread vertically from the sapphire/GaN or SiC/GaN interfaces up through the active region of LEDs, as shown in Fig. 2.7. These threading densities need to be drastically reduced because dislocations quench light emission of LEDs. These dislocation defects can be reduced by substrate patterning techniques such as Epitaxial Lateral Overgrowth, Pendeo Epitaxy, or Cantilever Epitaxy; above approaches rely on spatial filtering, terminating, and turning of threading dislocations, so they do not reach the device active region. In chapter 3 of this thesis, we report a novel structure of GaN LEDs grown on chemical wet

etching-patterned sapphire substrate (CWE-PSS) with a roughening surface consisted of V-shaped pits. Thus both the internal quantum efficiency and light extraction efficiency of LEDs can be enhanced simultaneously. The aim of this proposed structure is the reduction of TD defects by lateral overgrowth occurred on CWE-PSS and the increase of escape probability of emitting photons via the roughening surface.

2-2-2 Photon Extraction

In principle, 100% of the light could be extracted from an LED, but the current state-of-the-art light extraction efficiency is about 60%. Limitations in light extraction include total internal reflection at interfaces and light absorption within the device or in the packaging. Some light-extraction methods are shown in Fig. 2.8 and discussed in following.

Chip shaping has been used to increase light extraction from LEDs. Lumileds used an inverted pyramid shape to boost light output from a red (AlGaInP) LED to achieve wall-plug efficiency as high as 50% [2.5]. Cree has also used chip shaping to increase efficiencies in their commercial blue and green LEDs.

Surface texturing produces random scattering at the surface, increasing the likelihood that light will encounter a surface within its escape cone, thus increasing light extraction [2.7-2.8].

Photonic crystals can be used in multiple ways to increase light extraction efficiency. Two-dimensional (2D) photonic crystals can be used to scatter waveguided modes out of the active layer region. Another approach is to use 2D photonic crystals to change the photonic density of states in the active layer so that no in-plane modes are permitted. This would cause all emitted light from the quantum wells to be normal to the LED surface so that it would lie within the escape cone and not be reflected. A third possibility is to increase the internal quantum efficiency by enhancing the photonic density of states at the LED emission wavelength.
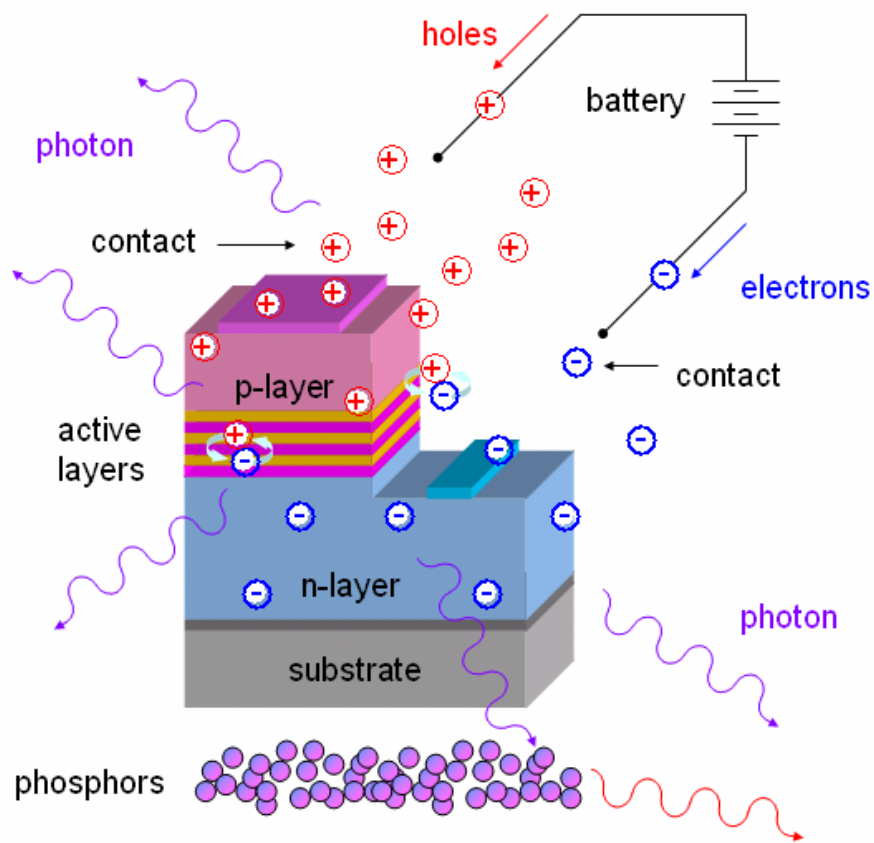
Fig. 2.1 A schematic of a generic LED structure illustrating the major stages in the photon life cycle from initial electrical energy from a battery to a mixture of photons that appears white to the human eye.
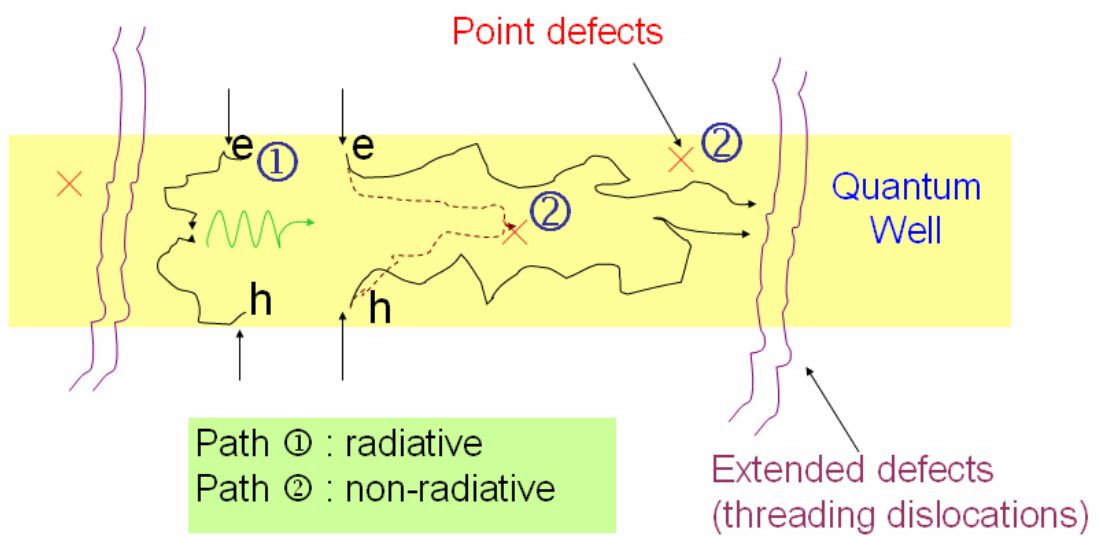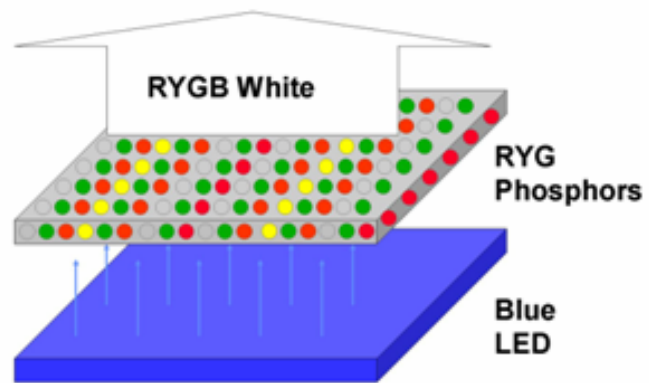
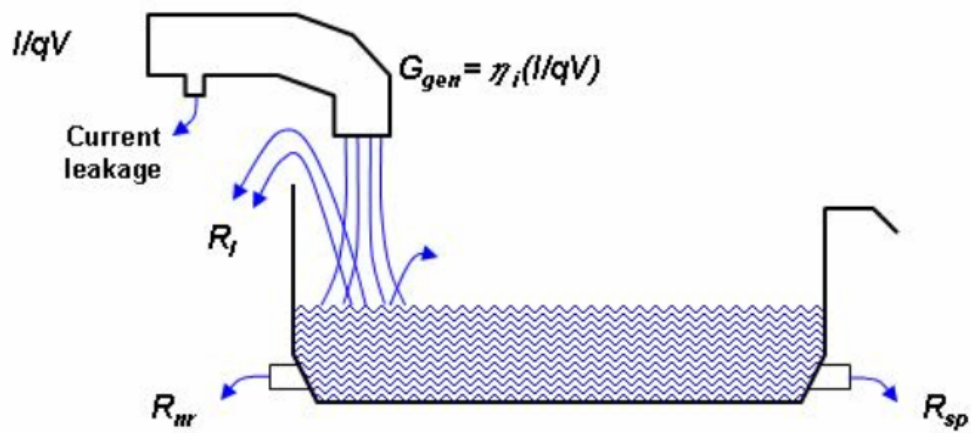**Fig. 2.2** Radiative and nonradiative recombination in materials.
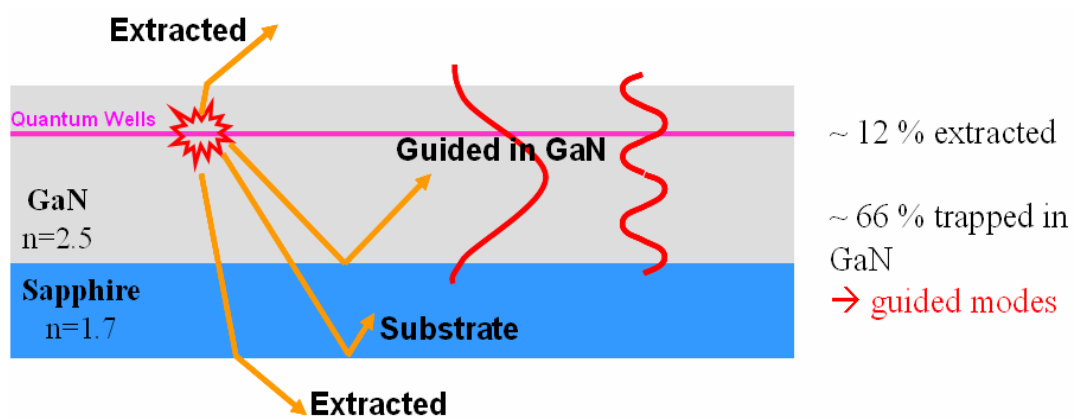
Fig. 2.3 Illustration of photons ray traces of conventional InGaN-based LEDs. Most photons (~66%) emitted from quantum wells are trapped inside LED chips, and only 12% photons can be extracted outside LEDs.
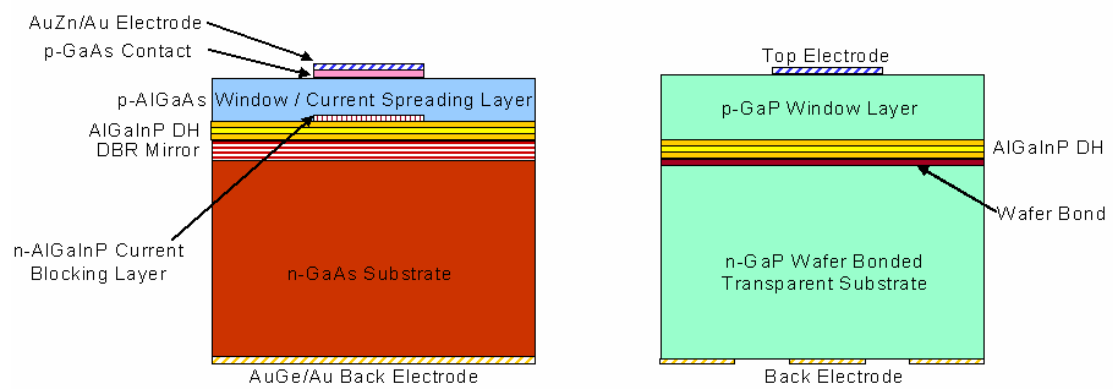
Fig. 2.4 Schematic illustration of the main approach to producing white light form monochromatic LEDs

Fig. 2.5 Schematic analogy of carriers injected into active regions and depletion through radiative, nonradiative, and leakage recombinations.

Fig. 2.6 AlGaInP LED with DBR mirror for improved light extraction and AlGaInP LED wafer-bonded to transparent GaP substrate.
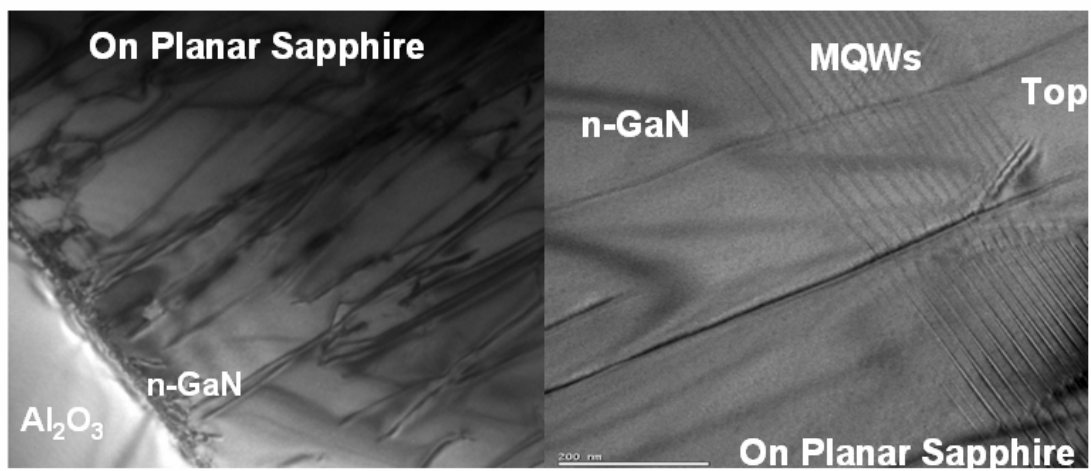
Fig. 2.7 SEM images of GaN material grown on sapphire substrate. Bunches of dislocation defects vertically thread from sapphire/GaN interface into active regions.
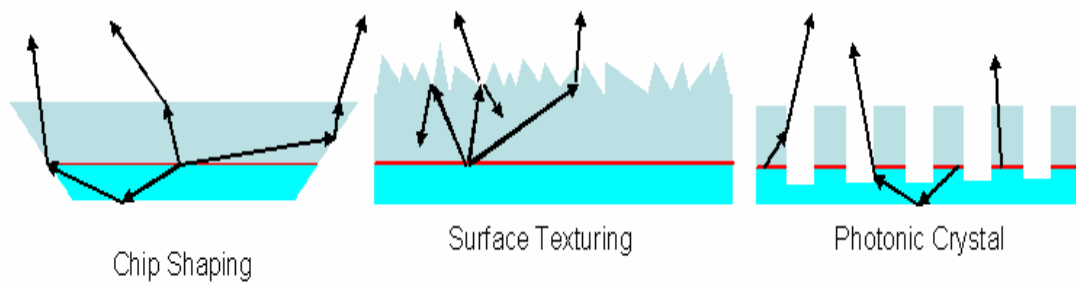
Fig. 2.8 Some LED light extraction schemes.

References of Chapter 2

[2.1] Ambacher, O., J. Majewski, C. Miskys, A. Link, M. Hermann, M. Eickhoff, M. Stutzmann, F. Bernardini, V. Fiorentini, V. Tilak, B. Schaff, and L. F. Eastman, "Pyroelectric Properties of Al(In)GaN/GaN Heteroand Quantum Well Structures," *J. Phys.: Condens. Matter* 14, 3399 (2002).

[2.2] Higashiwaki, M., T. Matsui, and T. Mimura, "AlGaN/GaN MIS-HFETs with fT of 163 GHz Using Cat- CVD SiN Gate Insulating and Passivation Layers," *IEEE Electron Device Letters* 27, 16 (2006).

[2.3] Mueller-Mach, R., G. Mueller, M. R. Krames, H. A. Hoppe, F. Stadler, W. Schnick, T. Juestel, P. Schmidt, "Highly Efficient All-Nitride Phosphor-Converted White Light Emitting Diode," *Phys. Stat. Sol.* (a) 202, 9 1727 (2005).

[2.4] E. F. Schubert, *Light-emitting diodes,* (Second Edition, Cambridge University Press, Cambridge, U.K., 2006.).

[2.5] M. R. Krames, M. Ochiai-Holcomb, G. E. Höfler, C. Carter-Coman, E. I. Chen, I.-H. Tan, P. Grillot, N. F. Gardner, H. C. Chui, J.-W. Huang, S. A. Stockman, F. A. Kish, M. G. Craford, T. S. Tan, C. P. Kocot: Appl. Phys. Lett. **75** (1999) 2365.

[2.6] Yablonovitch, E., "Photonic Crystals: Semiconductors of Light," *Scientific American*, 47-55 (December 2001).

[2.7] I. Schnitzer and E. Yablonovitch, "30% external quantum efficiency from surface textured, thin-film light-emitting diodes," *Appl. Phys. Lett.*, vol. 63, pp. 2174–2176, 1993.

[2.8] Reiner Windisch et al, "40% Efficient Thin-Film Surface-Textured Light-Emitting Diodes by Optimization of NaturalLithography", IEEE TRANSACTIONS ON ELECTRON DEVICES, VOL. 47, pp 1492-1498, 2000.

Chapter 3 Fabrication and Performance of InGaN-based LEDs with Patterned Substrates

3-1 Introduction

With recent commercial success of GaN light-emitting-diodes (LEDs), the need of even higher power and efficiency blue LEDs is imminent for their wide application in illumination [3.1]. These GaN LEDs were grown heteroepitaxially onto dissimilar substrates, such as sapphire and SiC, because of difficulties in the growth of bulk GaN. Sapphire is the most commonly used substrate because of its relatively low cost. However, owing to the large mismatch of lattice constant and thermal expansion between epitaxial GaN films and sapphire substrates, GaN grown on planar sapphire substrates results in high density of dislocation defects (10^8-10^{10} cm^{-2}) [3.2]. The threading dislocation (TD) defects originate from the interface between GaN and sapphire, and then thread into multiple quantum wells (MQWs) active region. It is known that the internal quantum efficiency (η_{Int}) of LEDs is the ratio of the number of generated photons inside the MQWs to that of injected electron-hole pairs. With such amount of TD defects mentioned above existing in GaN LEDs, energy states close to the middle of the energy gap would be generated and a large portion of injected electron-hole pairs is trapped and recombined nonradiatively [3.3]. Therefore, η_{Int} deteriorates due to the existence of TD defects. Furthermore, even when the injected electron-hole pairs recombine radiatively, most generated photons fall outside escape cones by total internal reflection due to the large refractive index difference between GaN and epoxy or air [3.4]. Thus the light extraction efficiency ($\eta_{Extraction}$) of LED devices is restricted as well. The external quantum efficiency (η_{Ext}) is the ratio of the number of emitted photons outside the LED device to that of injected electron-hole pairs and is a useful physical parameter to evaluate LED performance. It is defined

as :

$$\eta_{Ext} = \eta_{Int} \cdot \eta_{Extraction} \qquad\qquad (3\text{-}1)$$

Thus to enhance LED performance and alleviate issues mentioned above, there are various approaches to either improve η_{Int} [3.5-3.8] or $\eta_{Extraction}$ [3.9-3.11]. However, few reports were published on enhancing LED performance by simultaneously improving η_{Int} and $\eta_{Extraction}$ [3.12-3.13].

In this chapter, we report the detail investigation results of GaN LEDs grown on chemical wet etching-patterned sapphire substrate (CWE-PSS) with a roughening surface consisted of V-shaped pits. The aim of this proposed structure is the reduction of TD defects by lateral overgrowth occurred on CWE-PSS and the increase of escape probability of emitting photons via the roughening surface. In section 3-2 we present the detail fabrication of three LED devices that are used for comparison in this chapter. The V-shaped pits roughening surface is investigated by using scanning electron microscope (SEM) and transmission electron microscopy (TEM) in section 3-3-1. The paraboloidal autocorrelation function theoretically modeling the V-shaped pits roughening surface is also given in this section and demonstrates that this roughening surface performs as a strong diffuser. In section 3-3-2, we investigate the mechanism responding for improvement of the η_{Int} of the LED grown on CWE-PSS. TEM is used to inspect the crystallography and TD defects of LED devices. The η_{Int} of LEDs is measured by using temperature-dependent PL with variation of excitation power. In section 3-3-3, the optical diffraction of CWE-PSS is measured to study its efficiency as a trapped light extractor. The η_{Ext} of three LEDs is measured and the $\eta_{Extraction}$ of them is also derived based on the η_{Ext} and η_{Int} measured above. These results suggest that the LED grown on CWE-PSS combined with V-shaped pits on top surface is a promising approach to dramatically enhance light output power of GaN LEDs.

3-2 Fabrications of CWE-PSS and LED Devices

The SiO$_2$ film with hole-patterns of 3-μm-diameter and 4-μm-spacing was deposited onto the sapphire substrate by plasma-enhanced chemical vapor deposition (PECVD) to serve as the wet etching mask. Here we use a mixed solution of sulfuric and phosphoric acids (H$_2$SO$_4$: H$_3$PO$_4$ = 2:1) to etch sapphire substrate at operating temperature of 300 ^{o}C. The wet-etching rate for sapphire substrates was about 1 μm/minute in this study and can be related to the H$_3$PO$_4$ composition and etching temperature [3.14-3.15]. Figure 3.1 and 3.2 show the SEM images of the patterned sapphire substrate of the etching time of 90s and 120s, respectively. In Fig.3.1, the crystallography-etched pattern of an (0001)-oriented sapphire substrate has a flat-surface of {0001} C-plane with a triangle-shape in the center. Surrounding the triangle-shape C-plane are three facets of {1-102} R-plane with an angle of 57° against the [0001] C-axis. However, due to the relative fast etching rate of C-plane than that of R-plane, the triangle-shape flat-surface of {0001} C-plane in the pattern center finally vanishes with the increase of etching time. As shown in Fig.3.2, the {0001} C-plane is disappeared and only {1-102} R-plane is observed on the CWE-PSS with the etching time of 120s. Figure 3.3 shows the evolution of CWE-PSS with the increase of sapphire etching time and the corresponding cross sectional of CWE-PSS with the increase of etching time is shown in Fig. 3.4. It should be noted that the diameter of the sapphire pattern also increases with the increase of etching time due to the side-etching effect; however, the period of the sapphire pattern keeps the same as 6-μm. Additionally, the high slope (57°) crystallography-etched facet of CWE-PSS is hard to fabricate by dry etching and it has been demonstrated that this inclined facet was crucial for improving light extraction efficiency [3.15]. In the beginning of this chapter, we keep the depth of etched holes being 0.5-μm first, and discuss the physical mechanisms of the LED grown on it. Figure 3.5 (a) shows a

top-view SEM image of CWE-PSS employed in this section.

The LED structures were grown on CWE-PSS by low-pressure metal-organic chemical vapor deposition. Trimethylgallium (TMGa), trimethylindium (TMIn) and ammonia (NH_3) were used as the Ga, In and N precursors, respectively, while biscyclopentadienyl magnesium (Cp_2Mg) and silane (SiH_4) were used as the p and n-type doping sources. The device fabrication process is as follows. Following growth of a GaN nucleation layer at 520 ^{o}C, a 1.5-μm undoped GaN buffer layer and a 2.5-μm Si-doped n-type (5 x 10^{17}cm^{-3}) GaN cladding layer were grown at 1050 ^{o}C. The active region consists of ten periods of 2.5-nm $In_{0.23}Ga_{0.77}N$ / 10-nm GaN MQWs structure with Si doping in GaN barriers and it was grown at 700 ^{o}C. Beneath the MQWs structure is a strain-relaxation layer with five periods of 2.5-nm $In_{0.1}GaN_{0.9}N$ / 20-nm GaN superlattice (SL). Finally, a 0.4-μm Mg-doped p-type GaN cladding layer was grown on top. Two different growth temperature of p-type GaN cladding layers, 1050 ^{o}C and 800 ^{o}C, were used in this study. At a low growth temperature of GaN layers (i.e., 800 ^{o}C), large number of V-shaped pits can be seen on the top surface of the LED surface [3.16]. During the growth of these p-type cladding layers, Cp_2Mg flow rate was adjusted at different growth temperature so as to achieve the same Mg doping concentration of about 3 x 10^{17}cm^{-3} in all these samples. The grown wafer was patterned with mesa size of 100 x 180 μm^2 by a standard photolithographic process and partially dry-etched down to the n-type GaN. A 300-nm-thick indium-tin-oxide (ITO) was deposited as a current spreading layer and Cr/Au were then deposited as n and p electrodes. For device comparison purpose, three different LED structures were fabricated. LED-A is the conventional LED, which was grown on planar sapphire substrate and has a flat surface morphology of p-type GaN grown on 1050 ^{o}C. LED-B was grown on planar sapphire substrate but has a roughened surface morphology of p-type GaN grown on 800 ^{o}C. LED-C was grown on CWE-PSS and also has a

roughened surface morphology of p-type GaN grown on 800 ^{o}C. Figure 3.5 (b), (c) and (d) show schematic diagram of the final structure of LED-A, LED-B, and LED-C, respectively.

3-3 Experimental Results and Discussion

3-3-1 V-shaped Pits Roughening Surface

The SEM was used to investigate the change of surface morphology of *p*-type GaN caused by growth temperature. Figure 3.6 shows SEM images of surface morphology of LED-A, LED-B, and LED-C. In Fig. 3.6 (a), it is clearly seen that the surface of LED-A is quite flat and contains very few hexagonal pits. These hexagonal pits are originating from the so called V-shaped pit in MQWs [3.17-3.19]. The strain induced by the lattice mismatch between InGaN and GaN layers and the reduction of surface mobility due to the relative low growth temperature (700 ^{o}C) in MQWs, acts as a driving force for the formation of the V-shaped pits in MQWs. The formation of V-shaped pits in MQWs is mainly to release high strain energy induced by heteroepitaxy of InGaN/GaN materials around TD defects. Thus the bottom of each V-shaped pit was always connected to a TD defect and the density of V-shaped pits in MQWs is equivalent to that of TD defects [3.17]. However, the subsequent growth of *p*-type GaN at 1050 ^{o}C completely fills the V-shaped pits in MQWs due to the sufficient surface mobility provided under such high growth temperature. Therefore, a flat *p*-type GaN surface was observed in Fig. 3.6 (a). For LED-B and LED-C, during growth of *p*-type GaN, we reduce the surface mobility of migrated Ga atoms by decreasing growth temperature to 800 ^{o}C. Due to the insufficient energy for Ga atoms to migrate to proper sites, the lateral growth rate of GaN will become smaller than vertical growth rate of GaN and the V-shaped pits profile was duplicated in *p*-type GaN as that in MQWs. Figure 3.7 (a) shows cross-sectional TEM image of LED-B. In

Fig.3.7 (a), lots of V-shaped pits in MQWs were observed and most bottoms of pits were connected to TD defects as mentioned before. In Fig. 3.7 (a), apex positions of V-shaped pits in MQWs and *p*-type GaN are almost the same. As further evidence, an enlarged cross-sectional TEM image focusing on MQWs of LED-B is shown in Fig. 3.7 (b). The apexes of both pits in MQWs and *p*-type GaN were penetrated and connected by TD defects. Therefore, for LED-B and LED-C, densities of V-shaped pits in the very top surface of *p*-type GaN are actually equivalent to that of TD defects. In this section, we applied above approach to fabricate a roughening surface and account for the density of TD defects for LED-B and LED-C. In Fig. 3.6 (b), the V-shaped pits are distributed randomly on the top surface of LED-B and its surface density was estimated to be 1.28×10^9 /cm^2. However, in Fig. 3.6 (c), the V-shaped pits are distributed mainly in ridge regions (outside hole-arrays patterns of CWE-PSS) and its density dramatically decreases in trench regions (within hole-arrays patterns of CWE-PSS). Thus for LED-C, the overall surface density of V-shaped pits is 3.62×10^8 /cm^2. It was 3.5 times smaller than that of LED-B, indicating a significant reduction of TD defects. We believe the reduction of TD defects is due to adopting CWE-PSS scheme. The detail will be explained later.

To examine the diffused power of V-shaped pits in *p*-type GaN, angular dependent radiation pattern is measured using a He-Ne laser, as shown in Fig. 3.8, and the result is shown in Fig. 3.9. According to Fig. 3.8, the He-Ne laser is incident normally from the backside (sapphire) of LED-B wafer and the transmitted power was measured from −80° to 80°. The measured result of LED-A wafer is also plotted in Fig. 3.9 for comparison. The calculated radiation pattern of LED-B wafer is also shown in Fig. 3.9 and is given by the paraboloidal autocorrelation function describing the wide angle scattering of V-shaped pits [3.20]:

$$\langle I \rangle = \cos\theta \cdot \pi \cdot \exp(-S_2^2) \cdot \begin{bmatrix} (\dfrac{\omega_1}{\lambda S_1})^2 \cdot \exp\left\{-(\dfrac{\pi\omega_1}{\lambda S_1})^2 \cdot \left[\sin^2\theta - 2\sin\theta\sin\theta_0 + \sin^2\theta_0\right]\right\} \\[2mm] + 2(\dfrac{S_2\omega_2}{\lambda})^2\left\{1 + (\dfrac{2\pi\omega_2}{\lambda})^2 \cdot \left[\sin^2\theta - 2\sin\theta\sin\theta_0 + \sin^2\theta_0\right]\right\}^{-3/2} \end{bmatrix} \qquad (3\text{-}2)$$

Where λ is the incident wavelength, θ_0 is the incident angle of emitting light, θ is the detected angle, and ω is the correlation length of the roughening surface. S is the rms phase delay and defined as:

$$S(\theta_0) = 2\pi\frac{\sigma_h}{\lambda}(\sqrt{n^2 - \sin^2\theta_0} - \cos\theta_0) \qquad (3\text{-}3)$$

Where σ_h is the rms roughness of roughening surface and n is the index of refraction of GaN material. According to Eq (3-2), the diffused behavior of V-shaped pits roughening surface corresponds to a paraboloidal autocorrelation function for the largest roughness component (S_1 and ω_1) with an exponential autocorrelation function for the second roughness component (S_2 and ω_2) [3.20]. The V-shaped pits roughening surface can be described perfectly with $S_2 = 0.26$, $\omega_2/\lambda = 1.7$, and $\omega_1/S_1\lambda = 0.31$ in Eq (3-2), as shown in Fig. 3.9.

It is also useful to compare the radiation patterns of LED-A and LED-B with that of idealized Lambertian diffuser, that is given by

$$\langle I \rangle = \frac{\cos\theta}{\pi} \qquad (3\text{-}4)$$

In Fig .3.9, the diffused power of LED-B is between that of idealized Lambertian diffuser and LED-A. At detected angle of 0 degree, the detected power of LED-B is

one order of magnitude smaller than that of LED-A. On the other hand, at large detected angle ($|\theta| > 25^{\mathrm{o}}$), the detected power of radiation pattern of LED-B is almost one order of magnitude larger than that of LED-A. That means the roughening surface of LED-B could diffuse light emitted from MQWs efficiently. The diffused surface is very useful for the consideration of photon extraction [3.10-3.11]; especially for GaN LEDs that the critical angle is only about $\sin^{-1} (1/2.4) \sim 25^{\mathrm{o}}$. To predict diffused radiation patterns of V-shaped pits emitted by light with the angle larger than the critical angle, $\theta_0 = \pm 30^{\mathrm{o}}$ and $\pm 60^{\mathrm{o}}$ are substituted in Eq (3-2) and the results is shown in Fig 3.10. In Fig. 3.10, strong diffused power is still observed, even though the incident angles of emitting light are larger than the critical angle, indicating that the V-shaped pits could be thought as a strong diffuser of guided light.

3-3-2 Transmission electron microscopy (TEM) images

Now we focus on investigations of the reduction of TD defects density and the improvement of η_{Int} for LED-C grown on CWE-PSS. To shed light on the origin of η_{Int} enhancement by CWE-PSS, we used TEM to investigate crystalline quality of LEDs grown on CWE-PSS (LED-C) and on planar sapphire substrate (LED-B). For the LED grown on planar sapphire substrate (LED-B), cross-sectional TEM images of the GaN/ sapphire interface and MQWs region are shown in Fig. 3.11 (a) and (b), respectively. Bunches of dislocation defect threads can be seen radiating vertically from the GaN / sapphire interface into the MQWs region. The crystallography of films on CWE-PSS (LED-C) is drastically different as depicted in Fig. 3.11 (c) and (d) which show cross-sectional TEM images of GaN/ sapphire interface and MQWs region of the LED grown on CWE-PSS (LED-C), respectively. As shown in Fig. 3.11 (c), a large number of stacking faults are present in the trench region. The formation of stacking faults could be due to the homoepitaxial lateral growth initiated from the

ridge region to cover the trench region during the initial growth of GaN buffer layer, leading to high crystalline quality over trench regions [3.21]. These stacking faults interact with the vertical threading dislocations and bend them horizontally [3.22]. Thus fewer threading dislocations can penetrate into the active regions, implying high crystalline quality of LED-C grown on CWE-PSS. This is also the reason why fewer V-shaped pits were observed on LED-C within trench regions of hole-arrays patterns, as shown in Fig.3.6 (c).

Besides, according to Fig.3.11 (d), the cross section becomes clearer in region close to the MQWs, indicating the reduction of stacking faults density there. Thus the stacking faults will not have negative impact for active region because they terminate beneath the MQWs. As further evidence, figure 3.12 (a) and (b) show enlarged TEM images of the SL / MQWs region of LED grown on planar sapphire substrate and CWE-PSS, respectively. In Fig.3.12 (a), the threading dislocation defects obviously penetrate through the SL / MQWs region into the upper p-type GaN cladding layer. These penetrating defects induce leakage paths for injected carriers that decrease internal quantum efficiency of LED device. In stark contrast, clear interfaces between well and barrier in MQWs are observed in Fig. 3.12 (b) without any interruption of threading dislocation defects. Therefore, for LED grown on CWE-PSS, injected carriers can recombine and generate light more efficiently in active region, as compared to LED grown on planar sapphire substrate.

3-3-3 Temperature-dependent Photoluminescence

To further investigate the improvement of η_{Int} for LED-C grown on CWE-PSS, the temperature-dependent PL was measured with varying of excitation laser power. Excitation-dependent PL measurement was carried out for LED-B and LED-C at 300 and 77 K by He-Cd laser (325-nm, 50-mW). The temperature-dependent PL system is

shown in Fig. 3.13. PL quantum efficiency was calculated by [3.23],

$$\eta_{PL} = C \frac{I_{PL} / E_{PL}}{I_{EX} / E_{EX}} \qquad (3\text{-}5)$$

Where I_{PL} and I_{EX} are PL and excitation intensities, respectively. E_{PL} and E_{EX} are PL photon energy and excitation photon energy, respectively. C is a constant affected by carrier injection efficiency by laser, light extraction and correction efficiency of PL, and does not depend on either excitation power density or measurement temperature. Figure 3.14 shows relative PL quantum efficiency for LED-B and LED-C. PL. Curves are normalized by the peak value at 77 K for both samples. As can be seen, the efficiency is strongly dependent on excitation power. Basically, light extraction efficiency does not depend on either injected carriers or temperature. Therefore, the efficiency curves measured at different temperatures in Fig. 3.14 infer η_{Int} of LED devices. According to Fig. 3.14, η_{Int} are ~ 55 % and 62 % for LED-B and LED-C, respectively. Comparing LED-B and LED-C, around 13 % enhancement in η_{Int} is due to the better crystalline quality of LED-C grown on CWE-PSS. It should be noted that both LED-A and LED-B were grown on planar sapphire substrate and the epitaxial structures are identical except for the growth temperature of p-type GaN. Basically, η_{Int} of LED is dominated by the crystalline quality and defect density in the MQWs, and the subsequent growth of p-type GaN above MQWs does not affect η_{Int} much. Therefore, it is reasonable that we assume η_{Int} of LED-A is same as that of LED-B, or is ~ 55 %. In addition to enhance η_{Int}, CWE-PSS can improve $\eta_{Extraction}$ as well.

3-3-3 Optical Diffraction of CWE-PSS

To explain the enhancement in light extraction by using CWE-PSS, far-field

optical diffraction by the CWE-PSS is measured using a He-Ne laser (beam spot size 2-mm) in experimental setup depicted in Fig.3.15 (a). The incident angle, θ_i, of the He-Ne laser is fixed at 50° and the detected angle, θ_d, is varied from −80 ° to 80 °. The measured angular spectrum of diffracted power by CWE-PSS is shown in Fig. 3.15 (b). The inset in Fig. 3.15 (b) is Fraunhofer diffraction pattern of CWE-PSS recorded at a distance of 40-cm from the sample. The brightest dot in the center of diffraction pattern corresponds to the principal maxima of diffraction, which is located at θ_d = −50°. Considering the grating equation, the relation between incident wavelength, λ, angle of incidence, θ_i, and angle of reflection of mth order, $\theta_R^{(m)}$, is given by [3.24],

$$m\lambda = d \ (sin\theta_i + sin\theta_R^{(m)}) \tag{3-6}$$

Where m is the order of diffraction and d (7-μm) is separation between two identical slits. We calculate $\theta_R^{(m)}$ of all different orders by using Eq (3-6), and find them to be consistent with the measured results in Fig. 3.15 (b). Thus CWE-PSS serves the function as a diffraction grating. The refractive index of GaN (n_{GaN}) and sapphire ($n_{sapphire}$) are 2.4 and 1.7, respectively. The critical angle of GaN / sapphire interface is equal to $\sin^{-1}$ (1.7 / 2.4) ∼ 45° and that of GaN / air interface is equal to $\sin^{-1}$ (1 / 2.4) ∼ 25°. Thus light emitted from MQWs with incident angle of 50° at either interface will be completely trapped inside the LED device and only light with incident angle within ± 25° can be extracted from GaN / air interface. From Fig. 3.15 (b), the total integrated diffraction power from CWE-PSS within the escape cone from −25° to 25 ° (**P**$_{CWE-PSS}$) on the plane of incidence is found to be 10 times larger than that from planar sapphire substrate (**P**$_{planar}$). Therefore, in addition to reducing the density of TD defects, CWE-PSS also serves as a diffraction grating that effectively diffracts a portion of guided-light into the escape cone and increases escape probability of

52

photons inside LED chip. It shall be noted that in real case, light propagates in GaN material, thus the optical wavelength (λ / n_{GaN}) is smaller than that in the air. Therefore, the smaller $\theta_R^{(m)}$ is obtained in Eq (3-6), indicating larger enhancement is expected since the integrated diffracted power within $\pm 25°$ increases as well.

Fig. 3.16 (a) and (b) shows optical microscope image of LED-B and LED-C operating at 1 mA. The corresponding EL intensity distributions of LED-B and LED-C are shown in Fig. 3.16 (c) and (d), respectively. The EL intensity observed from the LED-C clearly exceeded those from LED-B. It can be seen that there are many localized light-emitting dots on LED-C. According to Fig. 3.16 (a), these light-emitting dots locate in the trench region of CWE-PSS, indicating stronger EL efficiency in this region. For LED-B, its EL intensity distribution is relative uniform, without observable any localized light-emitting dots. The higher light-emitting dots emitting from the trench regions in LED-C is due to good crystalline quality in this region. In addition, such an enhancement could also be attributed as a consequence of the enhanced $\eta_{Extraction}$ of LED-C grown on CWE-PSS compared to LED-B grown planar sapphire substrate, due to the effect of optical diffraction from CWE-PSS as mentioned above.

The integrated output optical power vs. drive current (L-I curve) of LED-A, LED-B, and LED-C is shown in Fig. 3.17. The LED-C, grown on CWE-PSS and with V-shaped pits on top surface, produced much higher light output as compared with that of LED-A and LED-B under all our measurement condition. With injection current of 20-mA, it was found that electroluminescence (EL) peaks all occurred at around 465-nm for these LEDs since exactly the same MQW structure was used. With a 20-mA current injection, it was found that output powers without epoxy resin encapsulant were 5.8, 7.0, and 8.5 mW for LED-A, LED-B, and LED-C, respectively. The saturated current, defined as the current corresponding to the saturated output

power, of LED-C is 20 mA larger than that of LED-B. It is because of by adopting CWE-PSS scheme, more valid active regions without penetration of leakage paths are injected by carriers. Comparing LED-B to LED-A at 20 mA, about 20 % enhancement of output power was observed. As mentioned above, the η_{Int} of LED-A and LED-B are identical (~ 55 %), thus the main enhancement of output power is attributed to higher $\eta_{Extraction}$ benefiting from V-shaped pits. Comparing the output power of LED-B to that of LED-C at 20 mA, LED-C demonstrates ~ 20 % enhancement over LED-B. The enhancement is attributed not only to high crystalline quality in MQWs, but also to strong diffraction by CWE-PSS.

The external quantum efficiency (η_{Ext}) can be derived from L-I curve and its corresponding emitting wavelengths. Thus based on these measured η_{Int} and η_{Ext}, light extraction efficiency ($\eta_{Extraction}$) can be estimated. At an injection current of 20 mA, η_{Ext}, η_{Int}, and $\eta_{Extraction}$ for LED-A, LED-B, and LED-C are summarized in Table 3.1. The densities of TD defects for three samples are also listed in Table I. For LED-A, the density of TD defects is estimated by counting for etching pits density and it is the same as that of LED-B [3.25]. According to Table I, the η_{Ext} are estimated to be ~ 27.5 %, 33 %, and 40 % for LED-A, LED-B, and LED-C, respectively. Comparing LED-B to LED-A, the main enhancement of η_{Ext} is due to the 20 % enhancement of $\eta_{Extraction}$, benefiting from the roughening surface of V-Shaped pits, as mentioned before. Comparing LED-C to LED-B, ~ 12.7 % and 7.5 % enhancements were observed in η_{Int} and $\eta_{Extraction}$, respectively; thus ~ 20% overall enhancement was obtained in η_{Ext}. The main enhancements in η_{Int} and $\eta_{Extraction}$ are attributed to the reduction of TD density and the strong diffraction from CWE-PSS, respectively. Comparing LED-C to LED-A, ~ 12.7 % and 29 % enhancements were observed in η_{Int} and $\eta_{Extraction}$, respectively; thus an overall 45 % enhancement was obtained in η_{Ext}. Therefore, comparing to conventional LEDs, the LED structure adopting CWE-PSS

and V-shaped pits on top surface can simultaneously enhance η_{Int} and $\eta_{Extraction}$, resulting in a dramatic improvement of total output power.

3-4 Summary

In summary, we investigate the mechanism responding for performance enhancement of InGaN-based light-emitting-diode (LED) grown on chemical wet etching-patterned sapphire substrate (CWE-PSS) with V-Shaped pit features on the top surface. According to temperature-dependent photoluminescence (PL) measurement and the measured external quantum efficiency, the structure can simultaneously enhance both internal quantum efficiency and light extraction efficiency. Comparing to devices grown on planar sapphire substrate, the threading dislocation defects of LED grown on CWE-PSS are reduced from 1.28×10^9 /cm^2 to 3.62×10^8 /cm^2, leading to a 13 % enhancement in internal quantum efficiency. In terms of the theoretical computing of radiation patterns, the V-Shaped pits roughening surface can be thought of as a strong diffuser with paraboloidal autocorrelation function, increasing the escape probability of trapped photons and achieving a 20 % enhancement in light extraction efficiency. Moreover, according to the measurement of optical diffraction power, CWE-PSS demonstrated superior guided light extraction efficiency than that of planar sapphire substrate, thus an extra 7.5 % enhancement in light extraction efficiency was obtained. Therefore, comparing to the conventional LED, an overall 45 % enhancement in integrated output power was achieved.
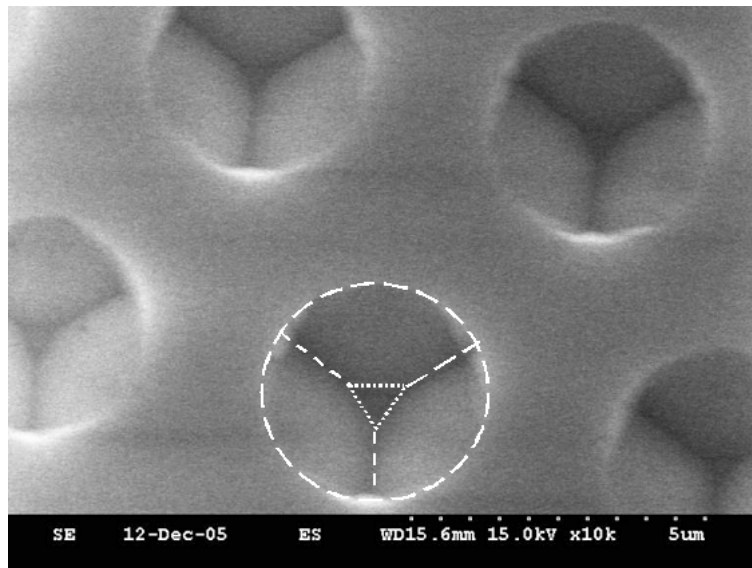
Fig.3.1 the SEM images of the CWE-PSS of the etching time of 90s.
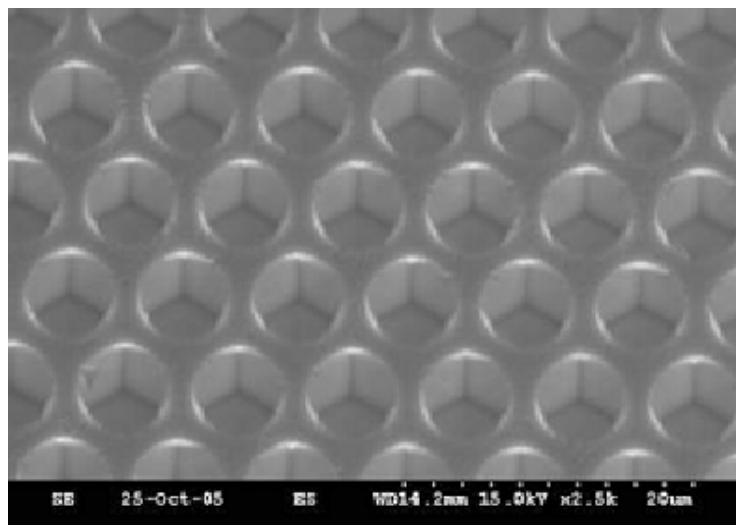
Fig.3.2 the SEM images of the CWE-PSS of the etching time of 120s.
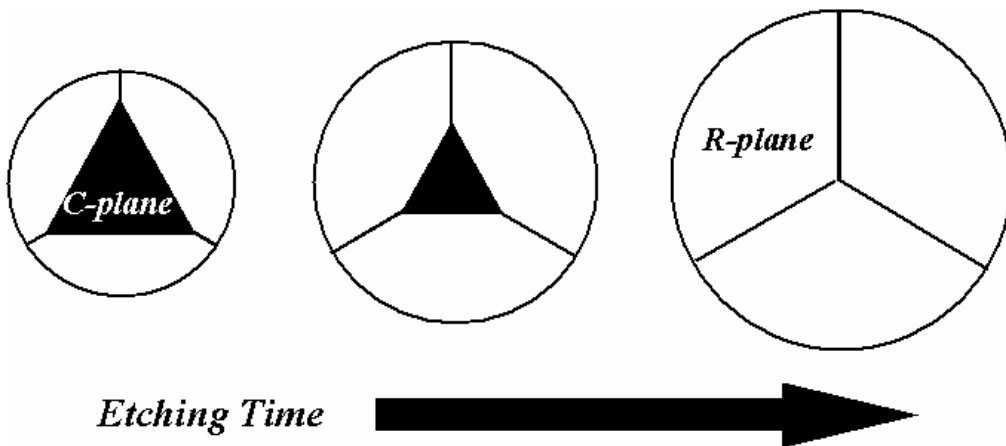
Fig.3.3 A top-view drawing depicts the evolution of CWE-PSS with the increasing of etching time.
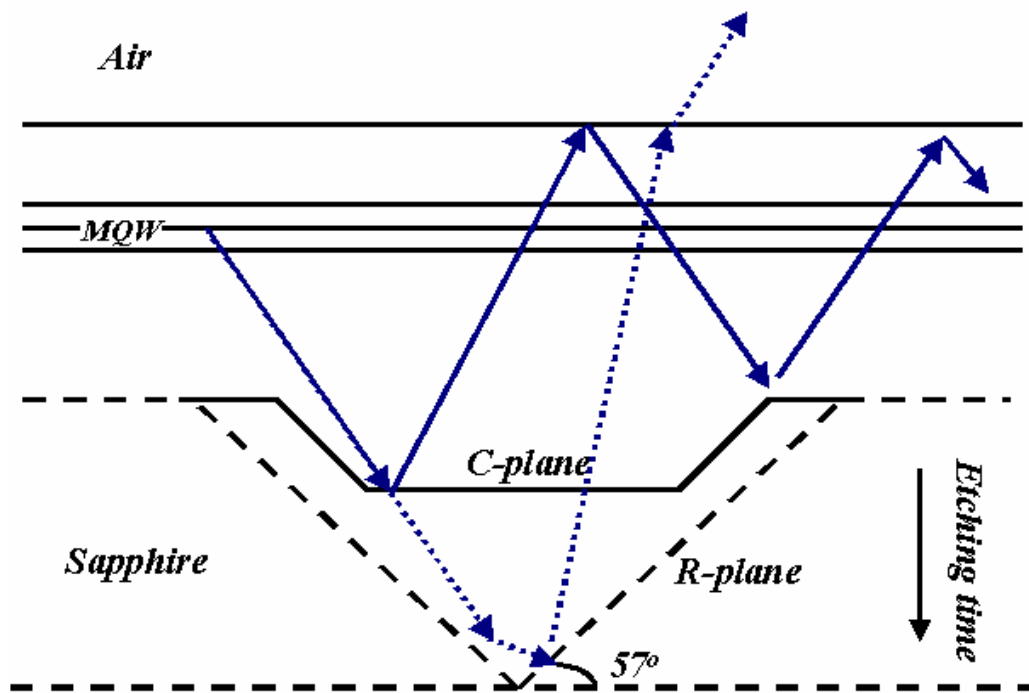
Fig.3.4 A schematic cross-sectional ray-tracing of the CWE-PSS LEDs with the increasing of sapphire etching time.
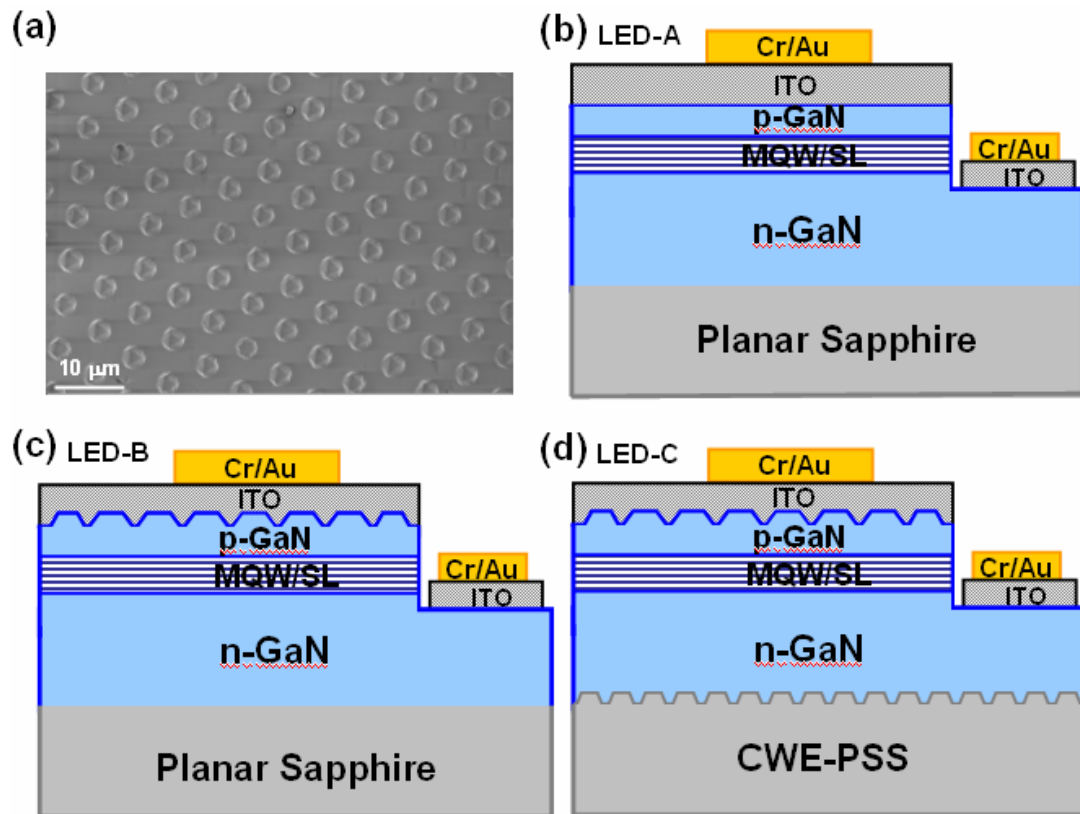
**Fig.3.5** (a) Top-view SEM image of CWE-PSS. (b), (c) and (d) show schematic diagram of LED-A, LED-B, and LED-C, respectively.
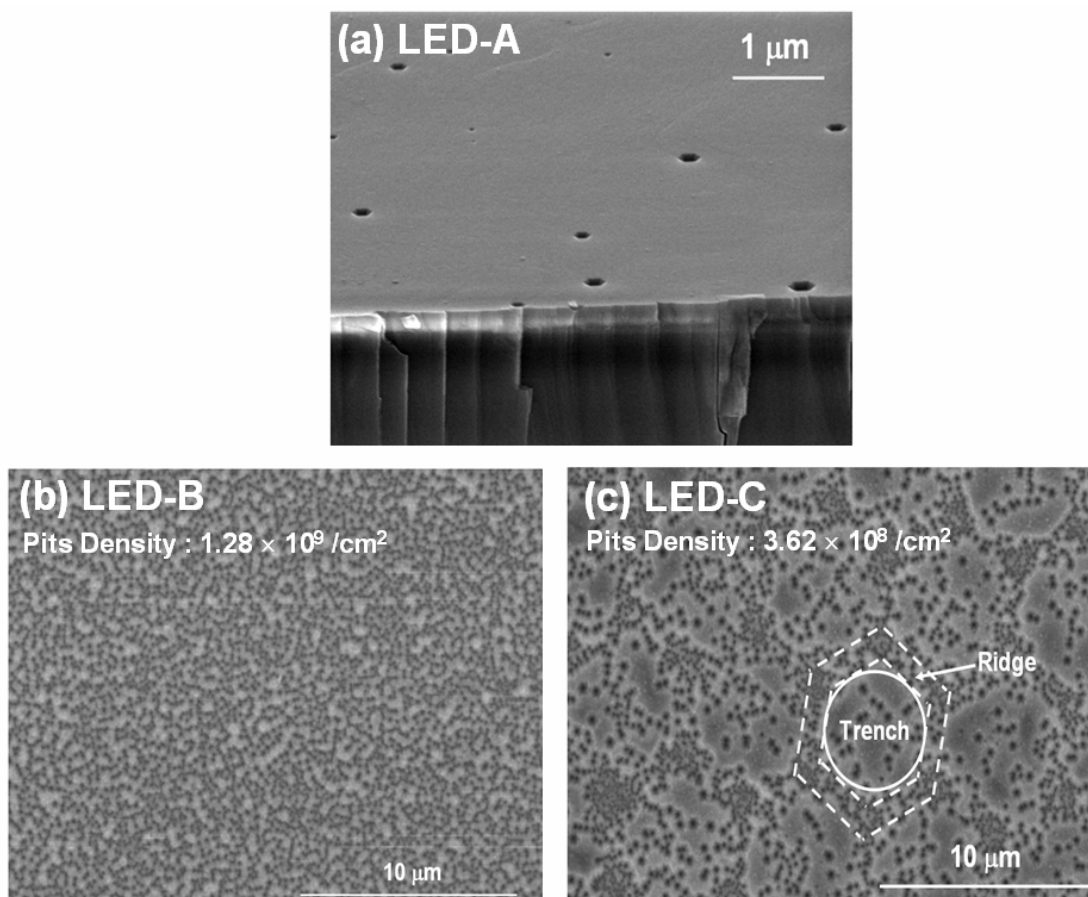
Fig. 3.6 Surface morphology SEM images of (a) LED-A, (b) LED-B, and (c) LED-C. Comparing (a) to (b), a large number of V-shaped pits were observed on the top surface of LED-B. In LED-C, most V-shaped pits (within hexagon mark) were observed in ridge regions of hole-arrays of CWE-PSS.
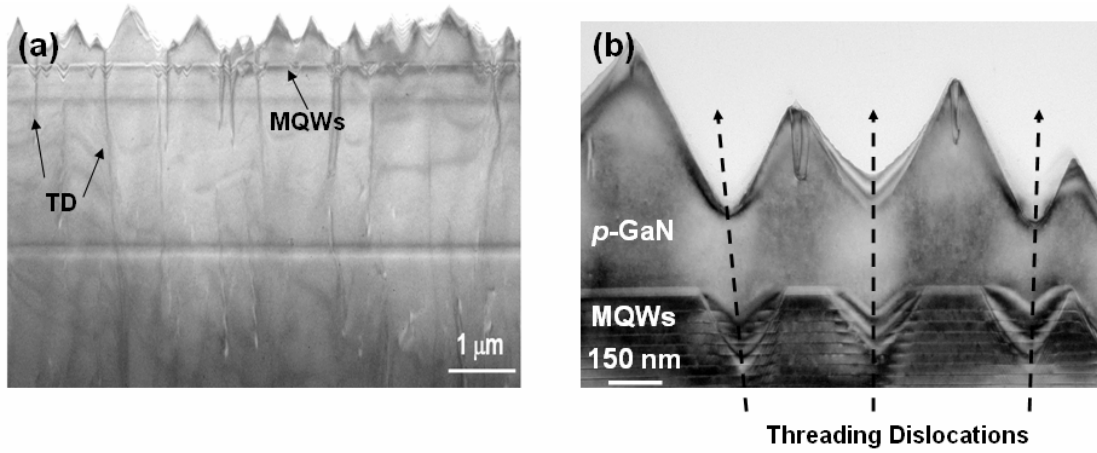
Fig. 3.7 (a) A cross-sectional TEM image of LED-B. (b) An enlarged cross-sectional TEM image focusing on MQWs of LED-B.
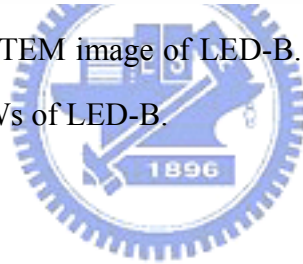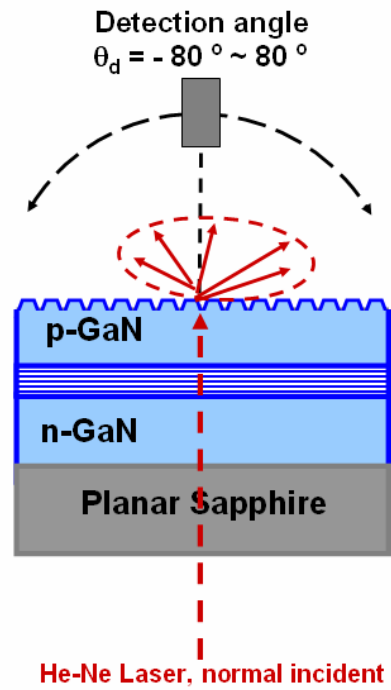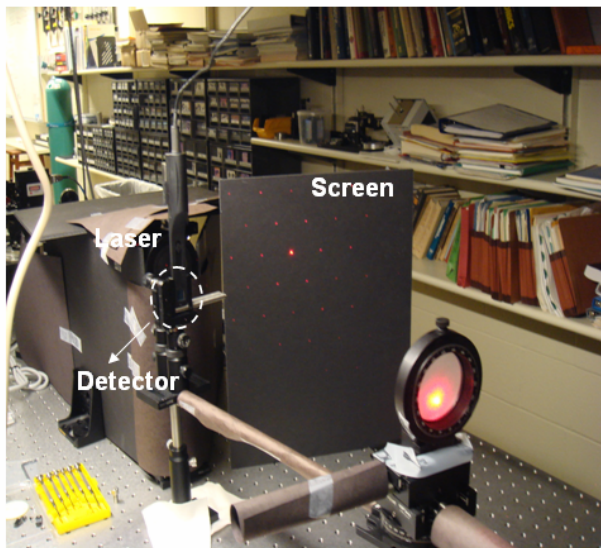
Fig. 3.8 Angular-dependent radiation pattern measurement system by using He-Ne laser beam at normal incidence.
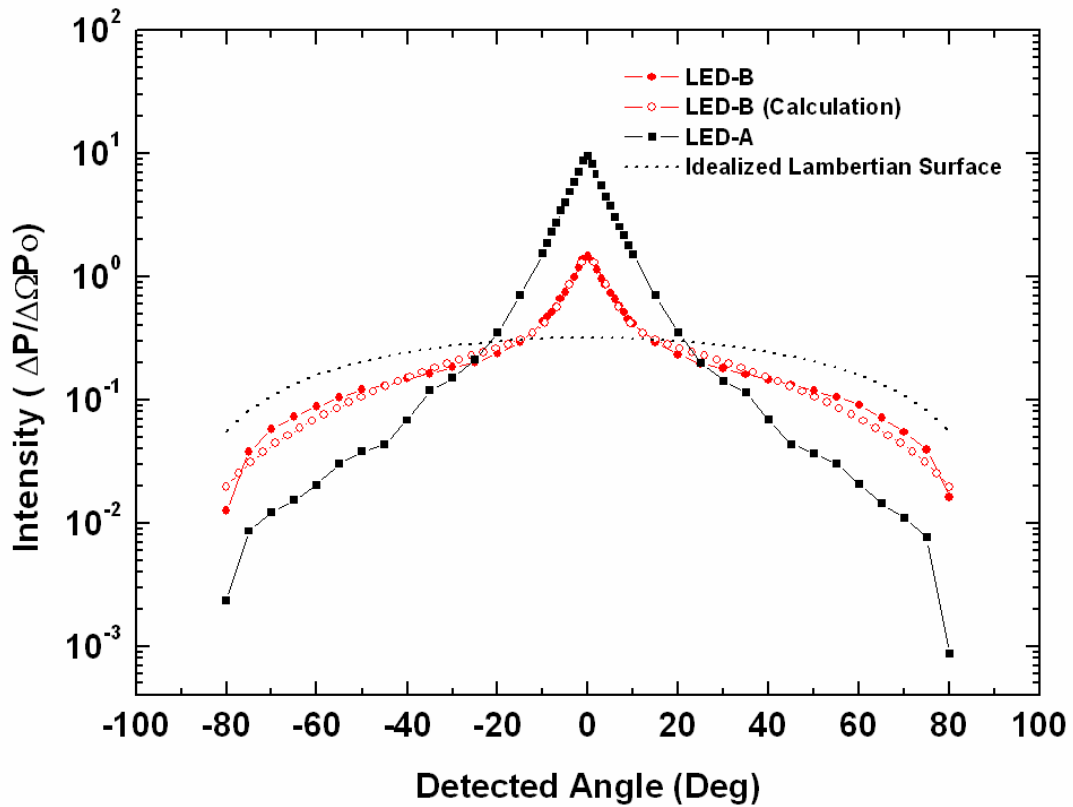
Fig. 3.9 Angular-dependent radiation pattern of flat surface (LED-A) and V-shaped pits roughening surface (LED-B) measured by using He-Ne laser beam at normal incidence. The radiation pattern of ideal Lambertian diffuser is also plotted for comparison (Dot line). The theoretical fitting of radiation pattern of LED-B is calculated using paraboloidal autocorrelation function.
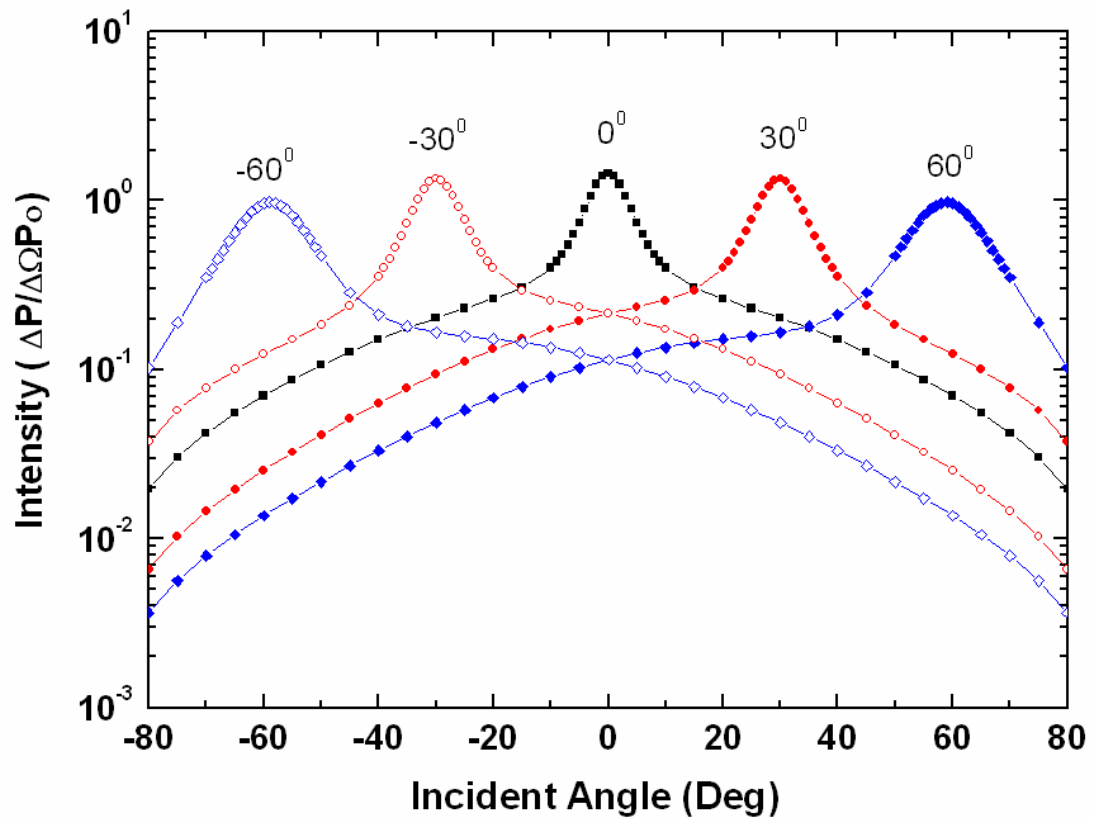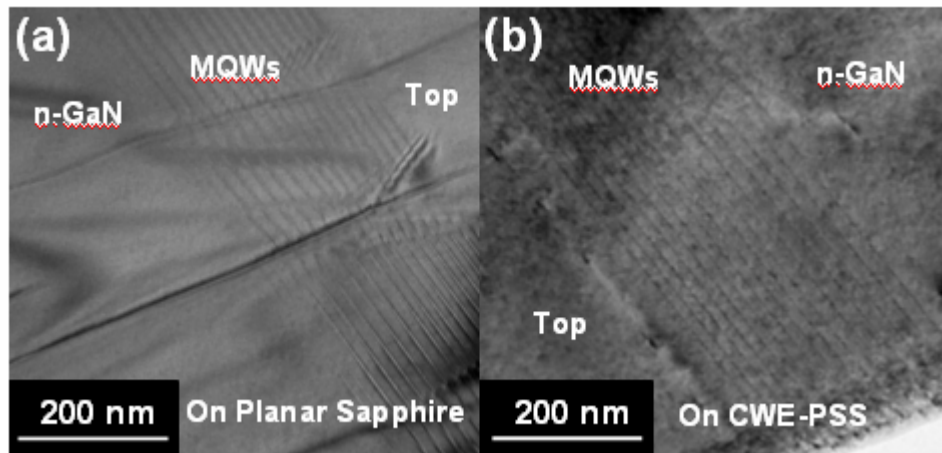
Fig. 3.10 The calculated radiation patterns of V-shaped pits roughening surface emitted by light with incident angle (θ_0) of 0°, $\pm 30^\circ$, and $\pm 60^\circ$.
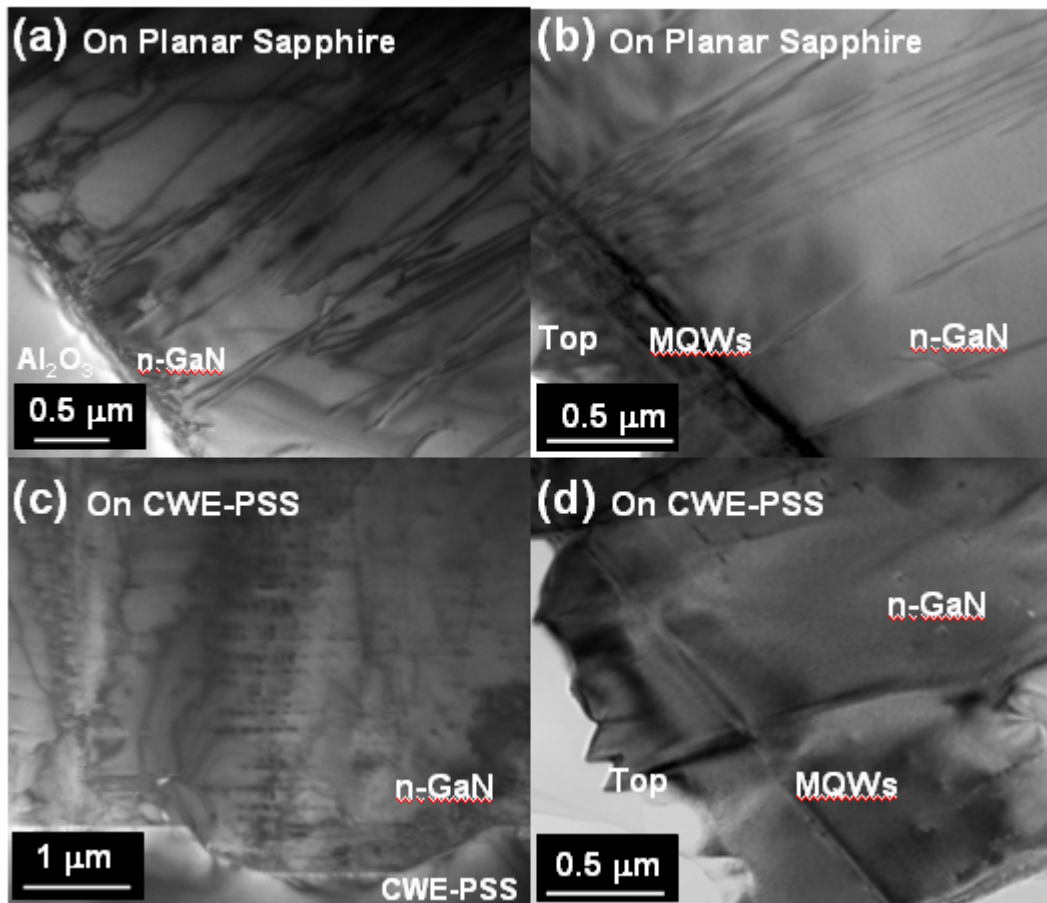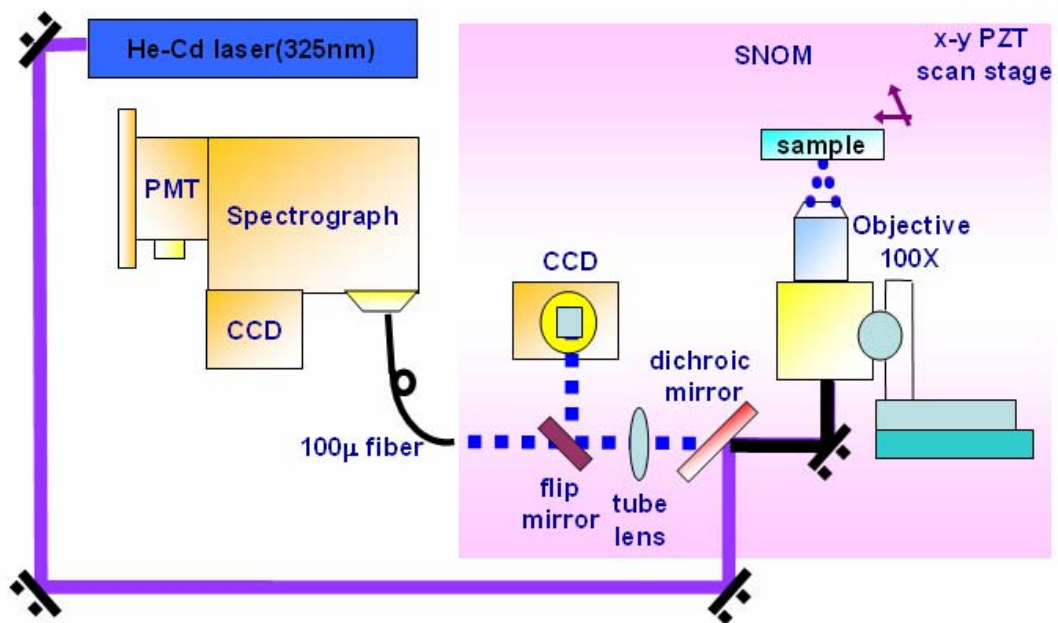
Fig. 3.11 Cross-sectional TEM images of GaN / sapphire interface grown on (a) planar sapphire substrate (LED-B) and (c) CWE-PSS (LED-C). Cross-sectional TEM images of MQWs region grown on (b) planar sapphire substrate (LED-B) and (d) CWE-PSS (LED-C).
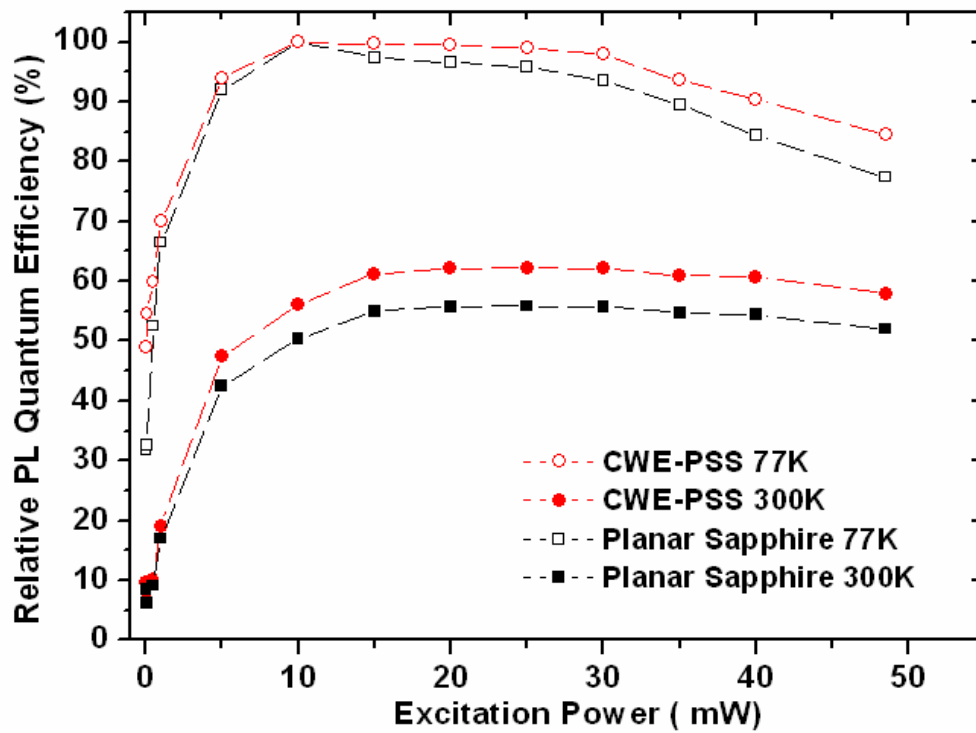
Fig.3.12 Enlarged TEM images of the SL / MQWs region of LED grown on (a) planar sapphire substrate (LED-B) and (b) CWE-PSS (LED-C).
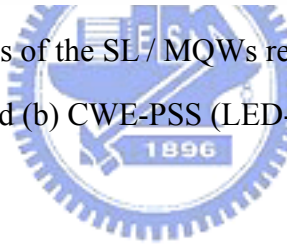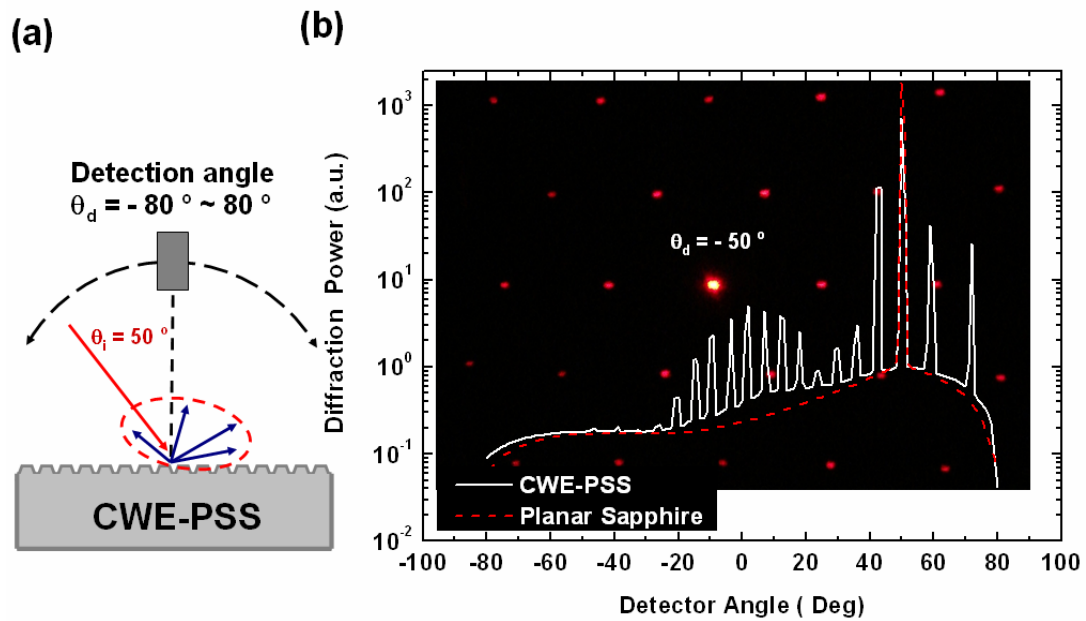
**Fig.3.13** Temperature-dependent PL system.

Fig.3.14 Relative PL quantum efficiency as a function of excitation power for LEDs grown on CWE-PSS (LED-C) and planar sapphire substrate (LED-B) measured at 77 and 300 K.

Fig. 3.15 (a) Experimental setup for measuring optical diffraction by CWE-PSS. (b) Measured angular dependence of diffraction power by CWE-PSS, inset in Fig. 3.15 (b) is measured Fraunhofer diffraction patterns of CWE-PSS.
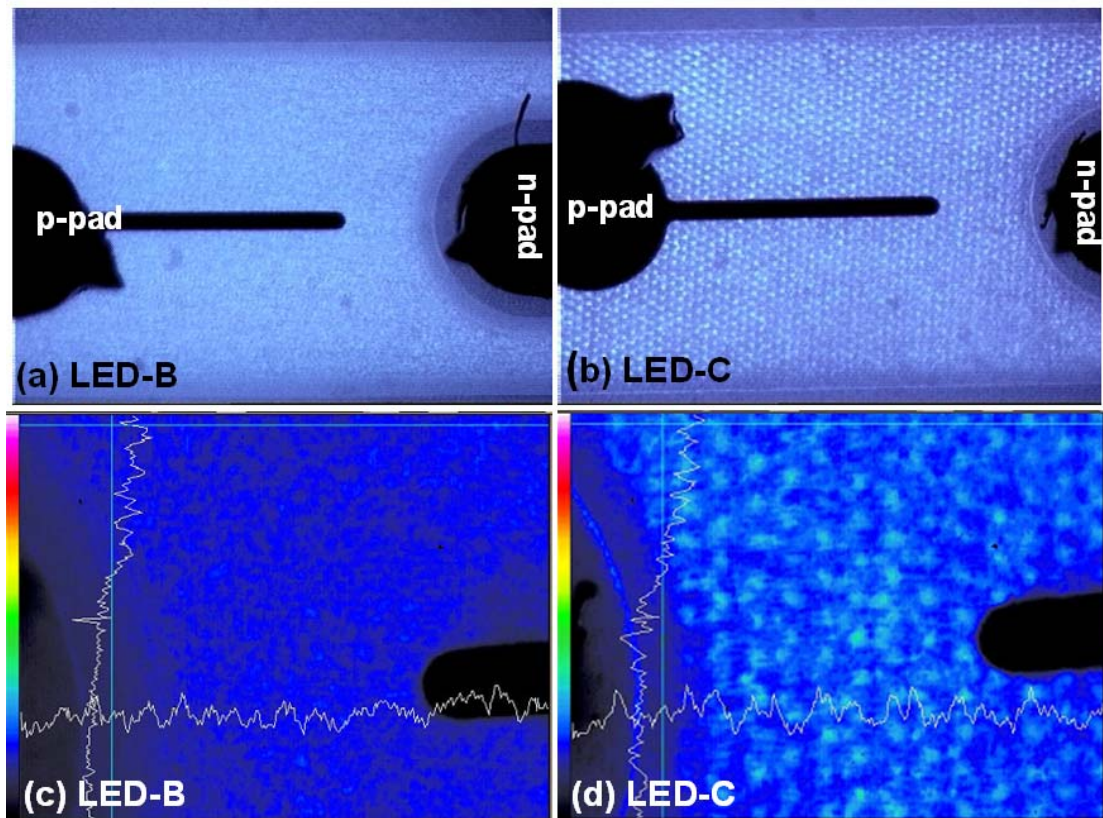
Fig. 3.16 Optical microscope images of (a) LED-B and (b) LED-C operating at 1 mA. EL intensity distributions of (c) LED-B and (d) LED-C.
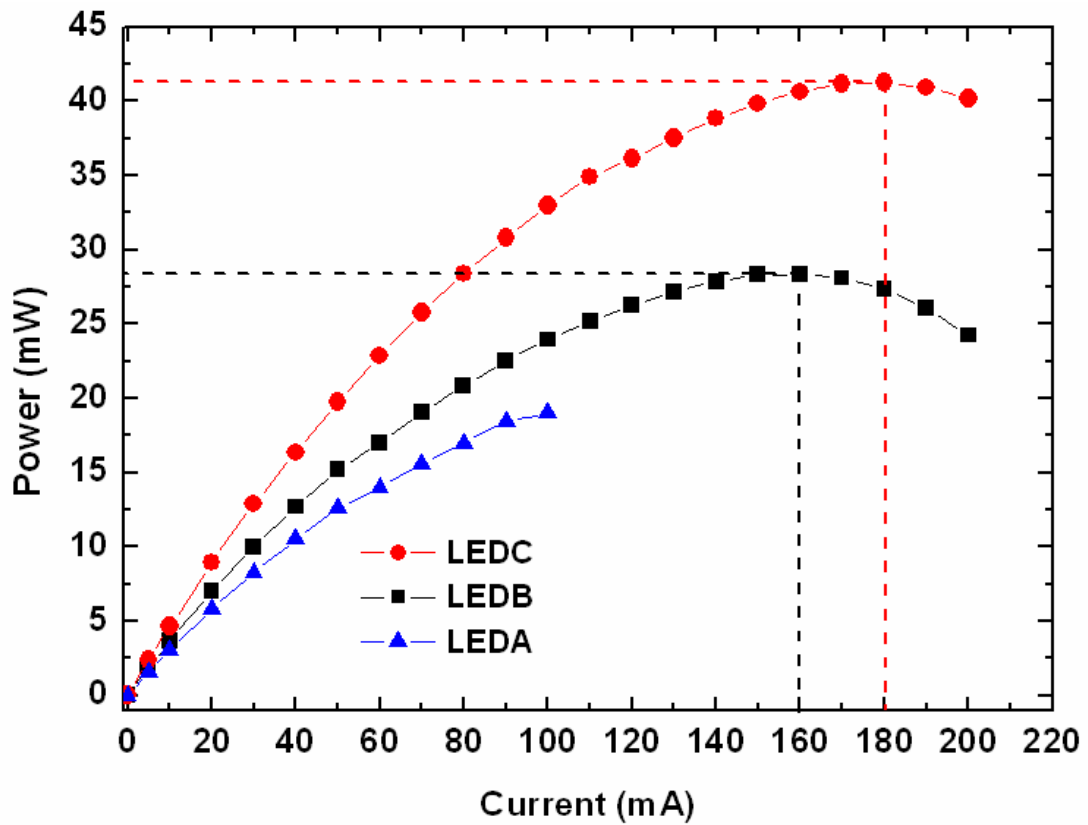
Fig. 3.17 The integrated output optical power vs. drive current (L-I curve) of LED-A, LED-B, and LED-C.

Substrate	LED-A	LED-B	LED-C
Measured External quantum efficiency (η_{Ext})	27.5%	33%	40%
Measured internal quantum efficiency (η_{Int})	55%	55%	62%
Calculated light extraction efficiency ($^*\eta_{Extraction}$)	50%	60%	64.5%
Dislocation Density (/cm^2)	1.28×10^9	1.28×10^9	3.62×10^8

$$^*\eta_{Ext} = \eta_{Int} \cdot \eta_{Extraction}$$

Table 3.1 Estimated η_{Ext} , η_{Int}, $\eta_{Extraction}$ and dislocation density of LED-A, LED-B, and LED-C at 20 mA current injection and temperature of 300 K.

References of Chapter 3

[3.1] S. Nakamura, S. Pearton and G. Fasol, The Blue Laser Diode: The Complete Story, 2nd ed. (Springer, Berlin, 2000).

[3.2] S. Nakamura, M. Senoh, S. Nagahama, N. Iwasa, T. Yamada, T. Matsushita, H. Kiyoku, Y. Sugimoto, T. Kozaki, H. Umemoto, M. Sano, K. Chocho, Appl. Phys. Lett., vol. 72, pp. 211–213, 1998.

[3.3] E. F. Schubert, *Light-emitting diodes,* (Second Edition, Cambridge University Press, Cambridge, U.K., 2006.).

[3.4] M. Broditsky and E. Yablonovitch, Proc. Spie, vol. 3002, pp119-122, 1997.

[3.5] Z. H. Feng and K. M. Lau, IEEE Photon. Technol. Lett., vol. 17, pp.1812-1814 2005.

[3.6] S. J. Chang, , Y. K. Su, Y. C. Lin, R. W. Chuang, C. S. Chang, J. K. Sheu, T. C. Wen, S. C. Shei, C. W. Kuo, and D. H. Fan, phys. stat. sol. (c) vol. 7, pp.2253–2256, 2003.

[3.7] D. S. Wuu, W. K. Wang, W. C. Shih, R. H. Horng, C. E. Lee, W. Y. Lin, and J. S. Fang, IEEE Photon. Technol. Lett. vol.17, pp. 288-290, 2005.

[3.8] Y.J. Lee, T.C. Hsu, H.C. Kuo, S.C.Wang, Y.L. Yang, S.N. Yen, Y.T. Chu, Y.J. Shen, M.H. Hsieh, M.J. Jou, B.J. Lee, Material Science and Engineering: B, V122, No. 3, pp184-187, 2005.

[3.9] T. Fujii, Y. Gao, R. Sharma, E. L. Hu, S. P. DenBaars, and S. Nakamura, Appl. Phys. Lett., vol. 84, pp. 855–857, 2004.

[3.10] J. K. Kim, H. Luo, Y. Xi, J. M. Shah, T. Gessmann, and E. F. Schubert, Journal of The Electrochemical Society, vol.153, pp. G105-G107, 2006.

[3.11] Y. J. Lee, T.C. Lu, H.C. Kuo, and S.C. Wang, IEEE Journal Of Quantum Electronics, vol. 42, , pp.1196-1201, 2006.

[3.12] Y. J. Lee, J. M. Hwang, T. C. Hsu, M. H. Hsieh, M. J. Jou, B. J. Lee, T.C. Lu, H.C. Kuo, and S.C. Wang, IEEE Photon. Technol. Lett. vol.18, pp. 132-1154, 2006.

[3.13] T.V.Cuong, H.S. Cheong, H.G. Kim. C.-H. Hong, E.K. Suh, H. K. Cho and B. H. Kong, Appl. Phys. Lett., vol. 90, pp. 131107, 2007.

[3.14] S. J. Kim, " Vertical Electrode GaN-Based Light-Emitting Diode Fabricated by Selective Wet Etching Technique," Jpn. J. Appl. Phys., vol. 44, pp. 2921-2924, 2005.

[3.15] S. J. Kim, "Improvement of GaN-Based Light-Emitting Diode by Indium-Tin-Oxide Transparent Electrode and Vertical Electrode," IEEE Photon. Technol. Lett. vol.17, pp. 1617-1619, 2005.

[3.16] S. J. Chang, L. W. Wu, Y. K. Su, Y. P. Hsu, W. C. Lai, J. M. Tsai, J. K. Sheu, and C. T. Lee, IEEE Photon.Technol. Lett., vol.6, pp1447-1449,2004.

[3.17] Y. Chen, T. Takeuchi, H. Amano, I. Akasaki, N. Yamada, Y. Kaneko, and S. Y. Wang, Appl. Phys. Lett., vol. 72, pp. 710-712, 1998.

[3.18] Ig-Hyeon Kim, Hyeong-Soo Park, Yong-Jo Park, and Taeil Kim, Appl. Phys. Lett., vol. 73, pp. 1634-1636, 1998.

[3.19] D. I. Florescu, S. M. Ting, J. C. Ramer, D. S. Lee, V. N Merai, A. Parkeh, D. Lu, E. A. Armour and L. Chernyak, Appl. Phys. Lett., vol. 83, pp. 33-35, 2003.

[3.20] L.G. Shirley and N. George, Applied Optics, vol. 27, pp. 1850-1861, 1988.

[3.21] Z.H. Feng, Y.D. Qi, Z.D. Lu, Kei May Lau, Journal of Crystal Growth. vol.272, pp. 327-332, 2004.

[3.22] Hyung Koun Cho, Jeong Yong Lee, Ki Soo Kim, Gye Mo Yang, Jae Ho Song, and Phil Won Yu, J. Appl. Phys. Vol. 89, pp.2617-2621,2001.

[3.23] S. Watanabe, N. Yamada, M. Nagashima, Y.Ueki, C. Sasaki, Y. Tamada, T. Taguchi, K. Tadatomo, H. Okagawa, and H. Kudo, Appl. Phys. Lett., vol. 83, pp. 4906-4908, 2003.

[3.24] Hermann A. Haus, *Waves and Fields in Optoelectronics*, (Prentice-Hall, Inc.,

Englewood cliffs, New Jersey). pp. 48.

[3.25] P. Visconti, K. M. Jones, M. A. Reshchikov, R. Cingolani, H. Morkoç, and R. J. Molnar, Appl. Phys. Lett., vol. 77, pp. 3532-3524, 2000.

Chapter 4 Phosphor-Free InGaN-based White LEDs by Using Laser Lift-off and Wafer-bonding Schemes

4-1 Introduction

As compared to conventional illumination technologies, high brightness indium gallium nitride (InGaN)-based light emitting diodes (LEDs) have a huge impact on the solid-state lighting (SSL) market, in terms of following key attributes: saturated color, small size, energy efficiency, robustness, and controllability [4.1]. There are many approaches to fabricate white LEDs [4.2-4.5]. Commercially available SSL sources are usually composed of InGaN LEDs, which function in the blue or UV wavelengths, and a combination of phosphors to produce a desired spectrum visible as white light [4.6]. However, the degradation of phosphor during the long period of optical pumping would deteriorate the output efficiency of this phosphor-converted white-light LED. By mixing two LED sources emitting complementary colors is another promising approach to obtain white light. Li et al. reveal the great potential of dichromatic light sources in terms of a very high luminous efficiency [4.7]. Their calculation shows that very high values of the luminous efficiency of 219 lm/W can potentially be reached, based on dichromatic white-light sources. A dual wavelength indium gallium nitride quantum well light emitting diode with three terminals has been reported in the literature by Ozden et al., where they inserted p^{++}/n^{++} InGan/GaN tunnel junction between separated blue and green active regions [4.8]. Although the presence of the tunnel junction in bottom device allowed for electrically isolated devices, typically added about 1 V to the forward voltage characteristics of the bottom device was observed. Besides, their dual-wavelength device is particularly for applications using fluorescence labeling of biological systems as diagnostic technique, no further discussion about the feasibility of SSL. Nicol et al. also employed tunnel junction to monolithically grow LEDs with two distinct wavelengths and used it to

excite two or more phosphors to produce white light [4.9]. According to their study, it is a fundamental trade-off between Mg concentration of p^+ GaN layer and its crystalline quality. In this report, we use wafer-bonding and sapphire laser lift-off techniques to fabricate InGaN-based dichromatic LEDs emitting at 470-nm and 550-nm, respectively. Thus conventional issue occurred often on using tunnel junctions, hardly to simultaneously achieving high Mg concentration and good crystalline quality on p^+ - layer, could be completely eliminated. Therefore, this novel and integrated structure could facilitate the early coming of SSL.

4-2 Laser Lift-Off and Wafer-Boding Techniques

The cross-section of dichromatic white LED is schematically shown in 4.1. Both blue and green epitaxial wafers used in this study were grown using a low-pressure metal-organic chemical vapor deposition (Aixtron 2600G) system onto C-face (0001) sapphire substrates. The blue LED layer-structure comprised a 30-nm-thick GaN nucleation layer, a 2-μm-thick undoped GaN layer, a 2-μm-thick Si-doped n-type GaN cladding layer, an un-intentionally doped active region of 470-nm emitting wavelength with five periods of InGaN/GaN multiple quantum wells (MQWs), and a 0.2-μm-thick Mg-doped p-type GaN cladding layer. Green wafer has almost the same epitaxial structure except for the active region, which also comprises five periods of InGaN/GaN MQWs but emitting with longer wavelength of 550-nm. Both p-side surfaces of blue and green wafers were deposited 300-nm-thick Indium-Tin-Oxide (ITO) for serving as transparent current-spreading layer. The blue wafer was flipped and then brought into contact with green wafer by benzocyclobutene (BCB) at the operating temperature of 220 ^{o}C. Here we have reduced the thickness of the BCB to as thin as 0.2-μm during the bonding process to minimize the impact of relative low thermal conductivity of BCB (~0.32 W/mK) on the overall device heat dissipation.

The bonded structure was then subjected to the laser-lift-off (LLO) process [4.10]. A KrF excimer laser at a wavelength of 248 nm with a pulse width of 25 ns was used to remove the sapphire substrate. The laser was incident from the backside of the sapphire substrate onto the sapphire/GaN interface to decompose GaN into Ga and N_2. After LLO, the subsequent processes involved sophisticated control of inductively coupled plasma (ICP). The fabrication of the dichromatic white LEDs with three-terminal device involved standard lithography and several etching steps to define mesa regions. The LED mesa has a 100-μm diameter hallow circle in the center for exposing of p-type contact region. Two dry-etching steps were required, to reach the blue LED's ITO current spreading layer and the n-type GaN layer of green LED, respectively. Part of insulated BCB bonding-layer sandwiched between ITO layers was removed by using O_2 plasma thus current from p-pad could be injected into ITO-layer on green LED and effectively spread. Metal for all three terminals was formed by Cr/Au and alloyed at 200 ^{o}C in N_2 atmosphere for 5 minutes. In order to further improve current-spreading of n-type GaN layers, both n-type metals of blue and green LEDs were designed with finger patterns. The top-view SEM image of final structure is shown in Fig. 4.2. The wafer was then cut into 480 μm x 480 μm chips and packaged into TO-18 without epoxy resin for subsequent measurements.

4-3 Experimental Results and Discussion

4-3-1 Optical Characteristic of Dichromatic Wavelengths

Figure 4.3 (a) shows plan view photograph of dichromatic LED. The blue and green LEDs share the same p-contact metal, thus emitting wavelength of the device can be chosen for either blue or green color by locating cathode-probe on n_1-pad or n_2-pad. For the simplest case of electric circuits, the device could be regarded as a parallel connection of blue and green LEDs. Figure 4.3 (b) and (c) show photographs while

turning on blue and green LEDs with injection current of 20 mA, respectively. Dark shadows on chip surfaces in both figures are due to the blocking of probes. According to this figure, by selectively probing the cathode terminal metals, the device can alternatively emit blue or green colors, revealing another potential application of the dichromatic LED for optical modulator [4.8]. Figure 4.4 shows the top view photograph of dichromatic white LED optical pumping by He-Cd 325-nm laser. In this figure, a strong white light composed of complementary dual-wavelengths is seen by human eye. The electroluminescence (EL) spectra while locating cathode-probe at n_1-pad (blue-emission) and n_2-pad (green emission) were shown in Fig.4.5 and Fig.4.6, respectively. In Fig. 4.5, a pure blue emission with emitting wavelength around 470-nm was observed. With increasing injection current up to 50 mA, peak position shifts toward to short wavelength (blue-shift) with shifting-rate of 0.18 nm/mA. This could be due to well-known quantum-confined stark-effect (QCSE). However, the shifting-rate reduced to about 0.089 nm/mA, while locating cathode-probe at n_2-pad, as shown in Fig. 4.6. Typically, the separation of electron and hole wave functions in band diagram was more severe for long-wavelength InGaN-based LEDs since more indium was incorporated into epitaxial structure, which induces stronger piezoelectric fields in quantum well region. Thus faster wavelength shifting-rate shall be observed for green LED. However, opposite behavior was observed in Fig.4.5 and Fig.4.6. We believe this could be attributed to the current-crowding effect on green LED. As shown in Fig.4.3 (c), current was crowded near p-pad region for green LED, which could raise junction temperature and lead red-shift for emitting wavelength. Therefore, as compared to Fig. 4.5, a slighter shifting-rate was observed in Fig. 4.6. The current-voltage (I-V curves) characteristic of blue, green and dichromatic white LEDs were shown in Fig.4.7. The series resistances are about 14 Ω and 17 Ω for blue and green LEDs, respectively. The higher series resistance of green LED was mainly

attributed to current-crowding effect, as mentioned above. The possible reason responsible for current crowding effect on green LED could be due to damage of the ITO current spreading layer. Before using ICP to dry etch green LED's mesa region, we used chemical wet etching to remove ITO current-spreading layer. The etching solution could leak and penetrate into chip sidewalls, thus damage part of ITO current-spreading layer on the top of green LED. This electrical characteristic issue could be overcome by further modifying process procedures. When we simultaneous located cathode-probes at n_1-and n_2 pads, the series resistance was reduced to about 12Ω. It is because the device could be regarded as a parallel connection of blue and green LEDs, series resistance of the device shall be reduced, as compared to every individual element in the electric circuit.

4-3-2 Luminous Efficiency of Dichromatic White Light LEDs

Figure 4.8 shows EL spectra of dichromatic white LEDs packaged on TO-18 with increase of injection currents. According to Fig. 4.8, below an injection current of 20 mA, a broad-band illumination of combination of blue and green colors could be observed. Then the blue peak becomes larger and dominates EL spectra when injection current is larger than 40 mA. Gaussian profiles are fitted to the two peaks of the EL spectra in Fig. 4.8 to determine the integrated emission intensity of the two emission bands. The integrated emission intensity versus injection currents, obtained from the EL measurements, is shown in Fig. 4.9. As compared to green emission, the larger increment in integrated EL spectra of blue emission with injection current was mainly attributed the better internal quantum efficiency of blue LEDs and the relatively uniform current spreading characteristic of ITO-layer on its p-type surface. Figure 4.10 shows the luminous efficiency (lm/W) and output power (mW) of dichromatic white LEDs with increasing injection current. The output power increases

linearly with injection current under all our measurement conditions, indicating good optical characteristic of the device. The luminous efficiency is 116 lm/W at 1 mA and rapidly drops to 40 lm/W at 20mA. Under such operating range (< 20mA), the corresponding EL illumination is quite broad of combination of blue and green colors, as shown in Fig. 4.8. In Fig. 4.10, the rapid decline of luminous efficiency with injection current is mainly due to follow-up domination of blue emission. As compared to green color, eyes are less sensitive to blue color, thus total integrated flux of the device is decreased with injection current and further reducing luminous efficiency. However, great potential for realizing SSL is successfully demonstrated by adopting this dichromatic lighting structure.

4-3 Summary

In summary, InGaN-based dichromatic-color blue/green (470-nm/550-nm) LEDs were well designed and successfully fabricated by using sapphire laser lift-off (LLO) and wafer-bonding schemes. Although current-crowding effect was observed on green LED due to artificial issue during process procedures, flat and broad EL spectra with combination of blue and green colors still emitted, accompanying with the luminous efficiency ranging from 116 to 40 lm/W (< 20mA). The rapid decline of luminous efficiency was due to the follow-up domination of blue emission with injection current. This integrated dichromatic lighting structure has a great potential to facilitate the early coming of SSL.
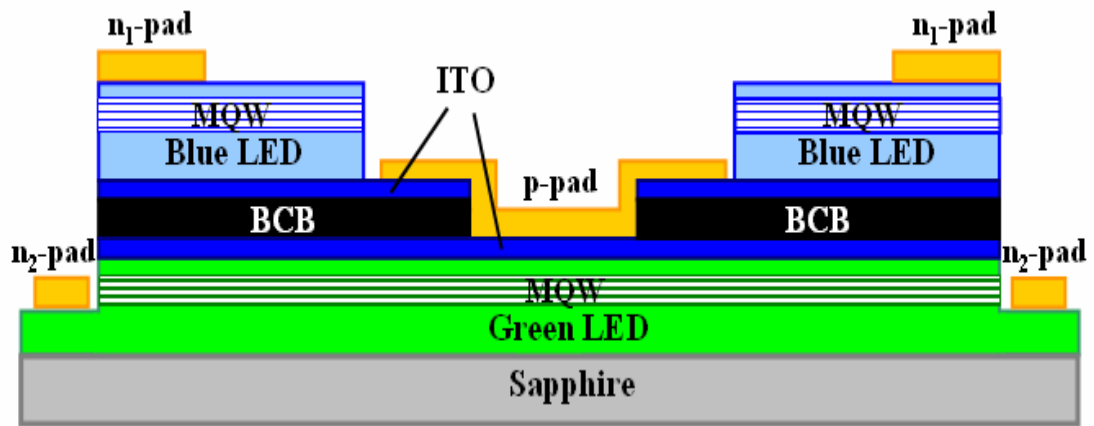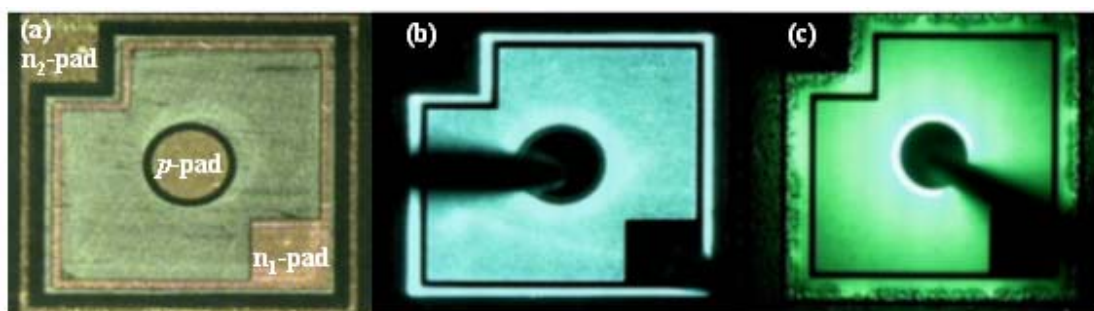
Fig.4.1 Schematic structure of InGaN-based dichromatic white LED by using laser lift off and wafer bonding schemes.
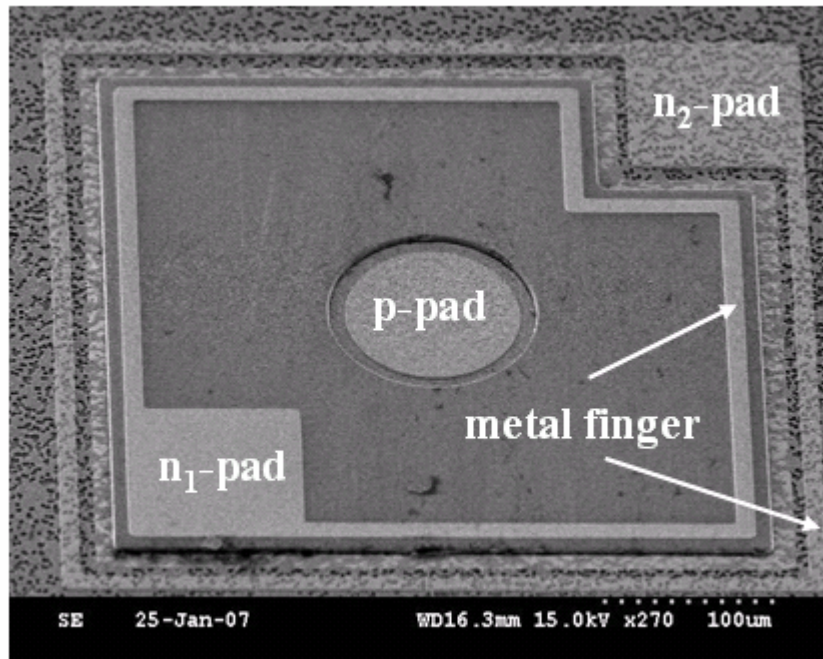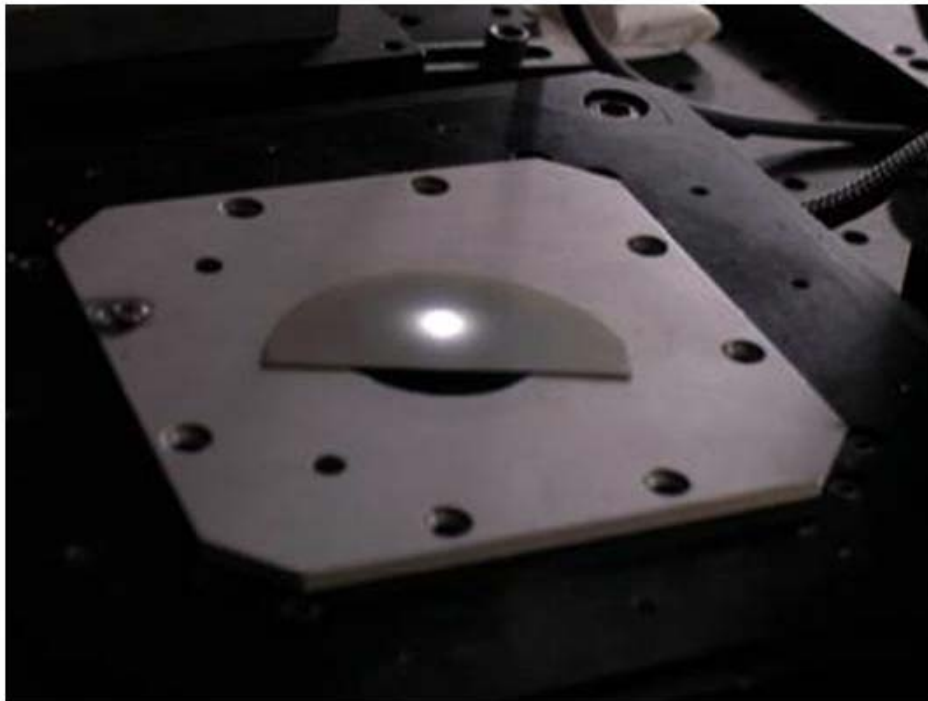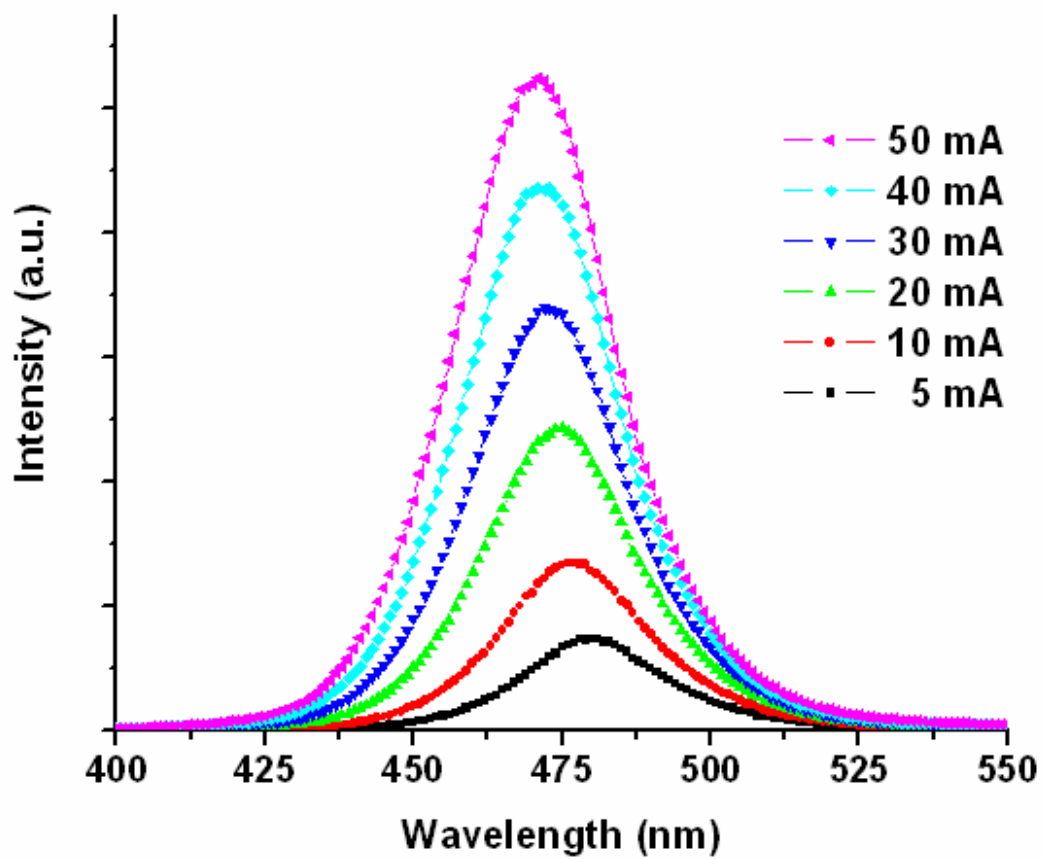
Fig.4.2 The top-view SEM image of phosphor-free dichromatic white light LEDs
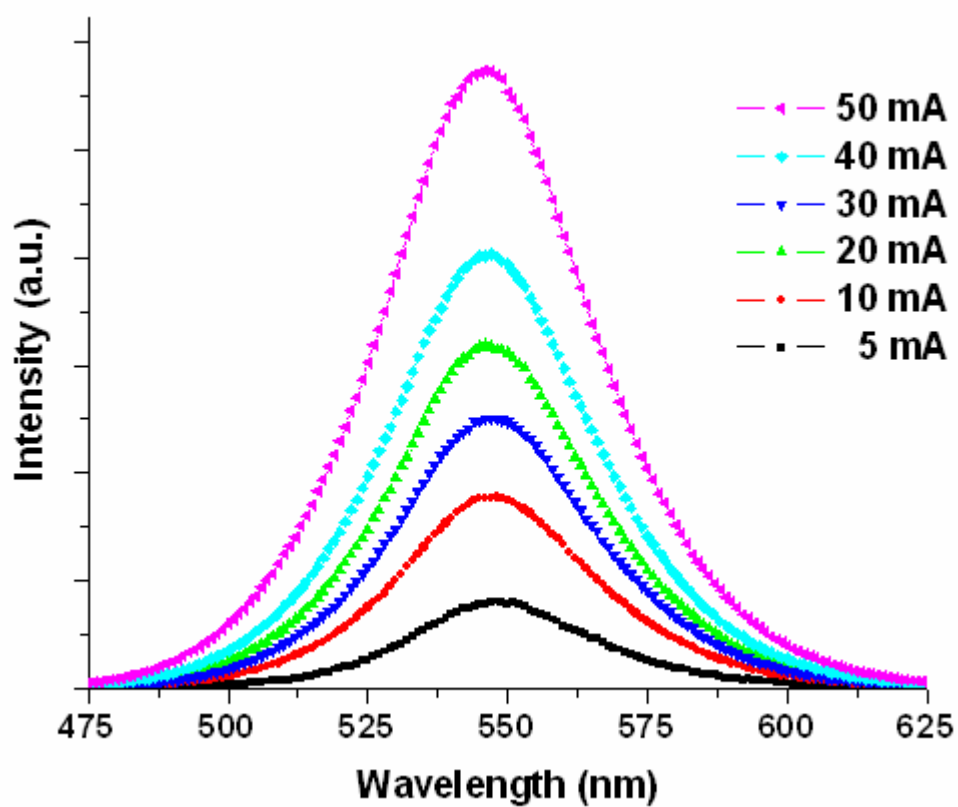
Fig.4.3 (a) Top view photograph of dichromatic white LED. (b) and (c) show photographs while turning on blue and green LEDs with an injection current of 20 mA, respectively.

Fig.4.4 Top view photograph of dichromatic white LED optical pumping by He-Cd 325-nm laser.
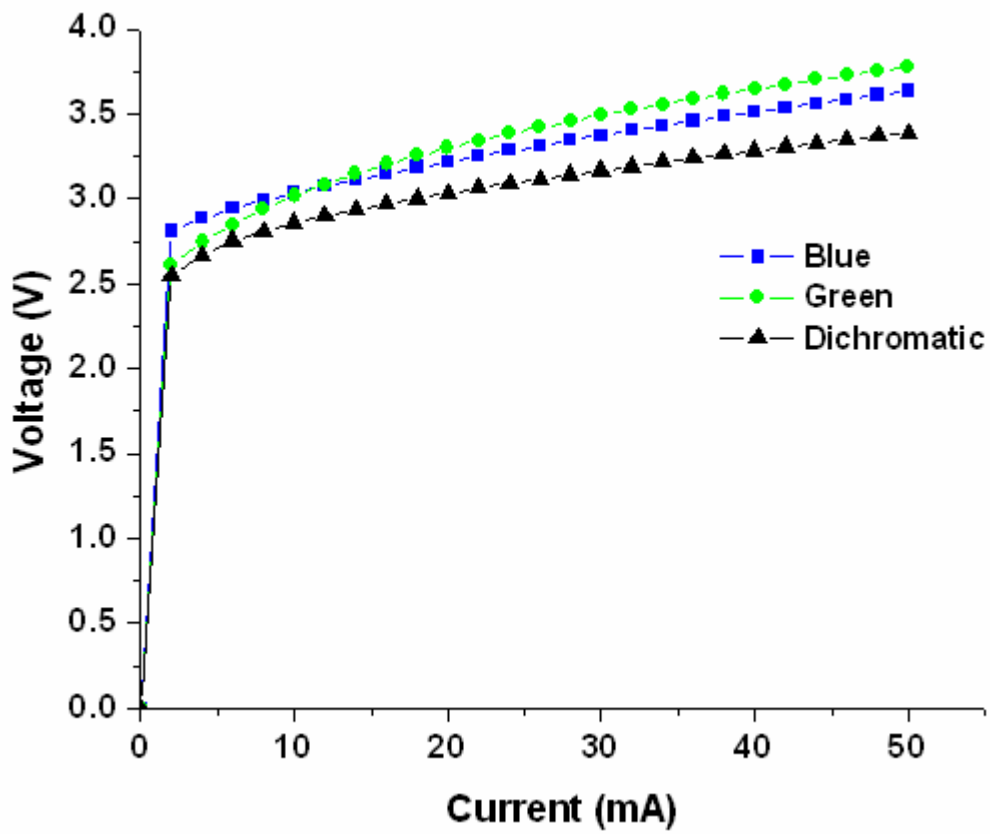
Fig. 4.5 The electroluminescence (EL) spectra while locating cathode-probe at n_1-pad (blue-emission)
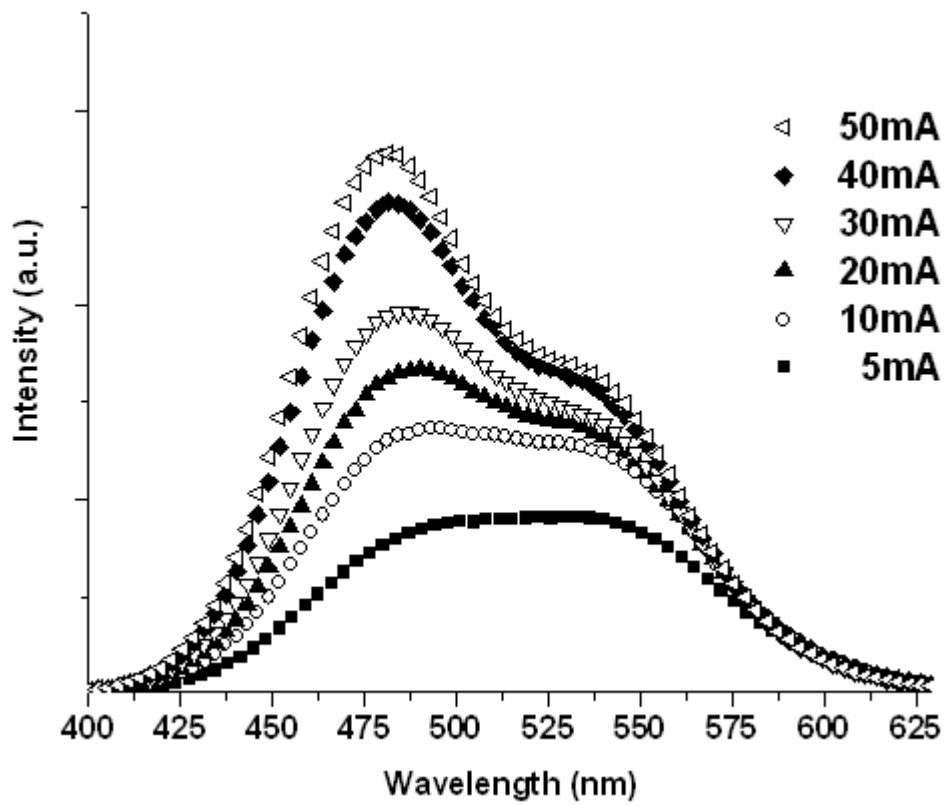
Fig. 4.6 The electroluminescence (EL) spectra while locating cathode-probe n_2-pad (green emission).
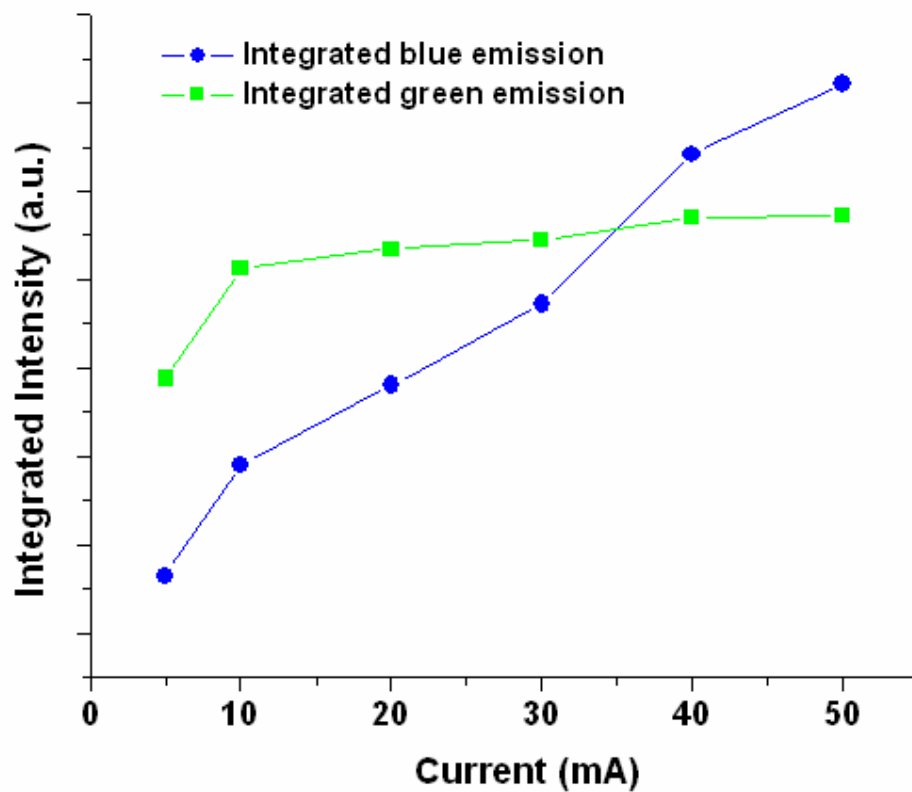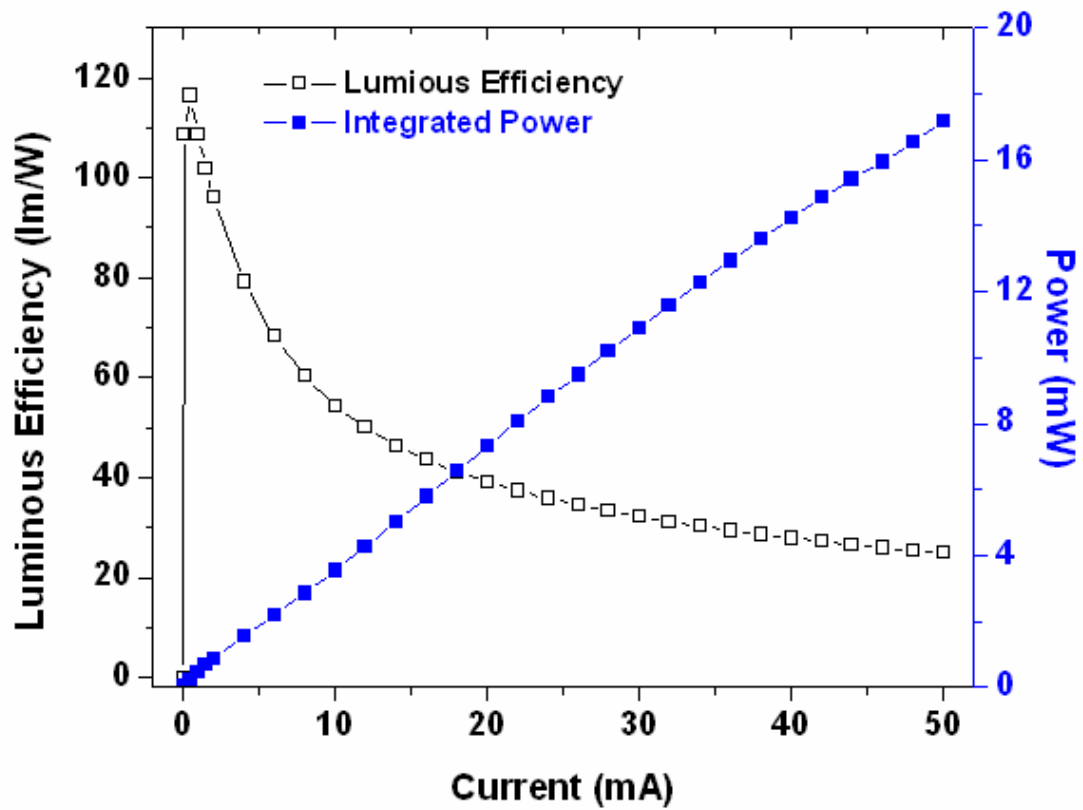
Fig. 4.7 The current-voltage (I-V curves) characteristic of blue, green and dichromatic white LEDs.

Fig.4.8 EL spectra of dichromatic white LEDs packaged on TO-18 with injection currents

Fig.4.9 The plot of integrated intensity vs injection currents at room temperature

Fig.4.10 The luminous efficiency and total output power of dichromatic white LEDs with injection current

References of Chapter 4

[4.1] E. F. Schubert, *Light-Emitting Diodes* (Cambridge University Press, Cambridge, U.K., 2003).

[4.2] S. C. Shei, J. K. Sheu, C. M. Tsai, W. C. Lai, M. L. Lee, and C. H. Kuo, "Emission mechanism of mixed-color InGaN/GaN multi-quantum-well light-emitting diodes," *Jpn. J. Appl. Phys.*, vol. 45, no. 4A, pp. 2463–2466, Apr. 2006.

[4.3] H.-S. Chen, D.-M. Yeh, C.-F. Lu, C.-F. Huang, W.-Y. Shiao, J.-J. Huang, C. C. Yang, I.-S. Liu, and W.-F. Su, "White light generation with CdSe-ZnS nanocrystals coated on an InGaN-GaN quantum-well blue/green two-wavelength light-emitting diode," *IEEE Photon. Technol. Lett.*, vol. 18, no. 13, pp. 1430–1432, Jul. 1, 2006.

[4.4] S. J. Chang, L. W. Wu, Y. K. Su, C. H. Kuo, W. C. Lai, Y. P. Hsu, J. K. Sheu, J. F. Chen, and J. M. Tsai, "Si and Zn co-doped InGaN-GaN white light-emitting diodes," *IEEE Trans. Electron Devices*, vol. 50, no. 2, pp. 519–521, Feb. 2003.

[4.5] Y. D. Qi, H. Liang, K. M. Lau, "Dual wavelength emission InGaN/GaN multi-quantum well LEDs grown by metalorganic vapor phase epitaxy," J. of Crystal Growth, vol. 272/1-4 pp. 333-340, 2004.

[4.6] R. Mueller-Mach, G. Mueller, M. Krames, and T. Trottier, "High-Power Phosphor-Converted Light-Emitting Diodes Based on III-Nitrides," IEEE J. Sel. Top. Quantum Electron. vol.8, pp.339-345, 2002.

[4.7] Y.-L. Li, Th. Gessmann, E. F. Schubert, and J. K. Sheu, "Carrier dynamics in nitride-based light-emitting p-n junction diodes with two active regions emitting at different wavelengths," *J. Appl. Phys.*, vol. 94, pp. 2167–2172, Aug. 2003.

[4.8] I. Ozden, E. Makaron, and A. V. Nurmikko, T. Takeuchi and M. Krames, "A dual-wavelength indium gallium nitride quantum well light emitting diode," . *Appl. Phys. Lett.*, vol. 79, pp. 2532–2534, 2001.

[4.9] David B. Nicol, Ali Asghar, Shalini Gupta, Hun Kang, Ming Pan, Martin Strassburg, Chris Summers, and Ian T. Ferguson, "Broadband spectrally dynamic solid state illumination source," phys. stat. sol. (c) vol.3, pp.2223–2226, 2006.

[4.10] J.T. Chu, T.C. Lu, H.H. Yao, C.C. Kao, W.D. Liang, J.Y. Tsai, H.C. Kuo and S.C. Wang, "Laser lift-off fabrication of blue-violet GaN-based vertical cavity surface emitting lasers optically pumped at room temperature", Jpn. J. Appl. Phys., V45, No.4A, pp2556-2560, 2006.

Chapter 5 Conclusion and Future Works

5-1 Conclusion

In this thesis, we have described novel designs of LEDs for solid-state-lighting application, including InGaN-based blue-color (470-nm) LEDs grown on chemical wet etching-patterned sapphire substrate (CWE-PSS) and complementary dual-wavelength (470-nm/550-nm) white-light LEDs combining with sapphire substrate laser lift-off (LLO) and wafer-bonding schemes.

We investigated physical mechanisms responsible for the dual enhancement in internal quantum efficiency and light extraction efficiency observed in InGaN-based LEDs grown on CWE-PSS. From TEM images, large number of stacking faults initiated from lateral growth of GaN buffer layer were observed in trench regions of CWE-PSS and effectively blocked penetration of threading dislocations. Thus the number of threading dislocations able to penetrate into the active region is reduced from 1.28×10^9 to 3.62×10^8 cm^{-2}, leading to a 12.7 % enhancement in internal quantum efficiency. Furthermore, measurement of optical diffraction by the CWE-PSS suggests that it also serves as a diffraction grating which diffracts portion of light trapped by total internal reflection into the escape cone, thereby improving light extraction efficiency by 7.5%.

InGaN-based dichromatic-color blue/green (470-nm/550-nm) LEDs were well designed and successfully fabricated by using sapphire LLO and wafer-bonding schemes. Although current-crowding effect was observed on green LED due to artificial issue during process procedures, flat and broad EL spectra with combination of blue and green colors still emitted, accompanying with the luminous efficiency ranging from 120 to 40 lm/W (< 20mA). The rapid decline of luminous efficiency was due to the follow-up domination of blue emission with injection current. This integrated dichromatic lighting structure has a great potential to facilitate the early

coming of solid-stating lighting.

5-2 Future Works

Although we have successfully demonstrated several impressive results as for the consideration of efficiency enhancement in visible-spectrum LEDs, there still has room to further improve performances of devices proposed in this thesis for the future works. Some suggestions for future works are as follows:

We use chemical wet etching to produce crystallography facet of {1-102} R-plane on sapphire substrate. Chemical wet etching is a quick, simple and feasible process for mass productions. However, the uniformity of etching profile is a critical issue once the process involved with chemistry solution. Thus the controllability and stability of chemistry etching environment and condition becomes an important segment for conducting this novel LED structure into industrial lines in the future.

Although the dichromatic-color white light LEDs can achieve luminous efficiency up to 120lm/W, the color rendering would be a critical issue if we want to employ this structure as lighting source. Additional phosphor-convention emitting red color would be necessary to improve the white light's quality for lighting application in the future.

PUBLICATION LIST

Journal Paper

1. **Y.J. Lee**, T.C. Hsu, H.C. Kuo, S.C.Wang, Y.L. Yang, S.N. Yen, Y.T. Chu, Y.J. Shen, M.H. Hsieh, M.J. Jou, B.J. Lee, "Improvement in light-output efficiency of Near-Ultraviolet InGaN–GaN LEDs Fabricated on Stripe Patterned Sapphire Substrates", *Material Science and Engineering: B, V122, No. 3, pp184-187, 2005.*

2. **Y. J. Lee**, H. C. Kuo, S. C. Wang, T. C. Hsu, M. H. Hsieh, M. J. Jou, and B. J. Lee "Increasing the extraction efficiency of AlGaInP LEDs via n-side surface roughening", *IEEE Photonic Technology Letter, Vol. 17, No. 11, pp2289-2291, NOVEMBER, 2005.*

3. **Y. J. Lee**, H. C. Tseng, H. C. Kuo, S. C. Wang, C. W. Chang, T. C. Hsu, Y. L. Yang, M. H. Hsieh, M. J. Jou, and B. J. Lee, "Improvement in Light-Output Efficiency of AlGaInP LEDs Fabricated on Stripe Patterned Epitaxy", *IEEE Photonic Technology Letter, Vol. 17, No. 12, pp2532-2534, DECEMBER, 2005.*

4. **Y. J. Lee**, T.C. Lu, H.C. Kuo, S.C. Wang, M. J. Liou, C.W. Chang, T. C. Hsu, M. H. Hsieh, M. J. Jou, and B. J. Lee, "AlGaInP LEDs with Stripe Patterned Omni-Directional Reflector", *Japanese Journal of Applied Physics, Vol. 45, Part 1, No. 2A, pp643-645, Feb. 2006 .*

5. **Y. J. Lee**, T.C. Lu, H.C. Kuo, S.C. Wang, M. J. Liou, C.W. Chang, T. C. Hsu, M. H. Hsieh, M. J. Jou, and B. J. Lee, "High brightness AlGaInP-based light emitting diodes by adopting the stripe-patterned omni-directional reflector", *Semicond. Sci. Technol. Vol.21, pp.184–189, 2006.*

6. **Y. J. Lee,** J.M.Hwang, T. C. Hsu, M. H. Hsieh, M. J. Jou, B. J. Lee, T.C. Lu, H.C. Kuo, and S.C. Wang, "GaN-based LEDs with Al-Deposited V-Shape Sapphire Facet Mirror," *IEEE Photonic Technology Letter, Vol. 18, No. 8, pp.724-726, March, 2006 .*

7. **Y. J. Lee,** J.M.Hwang, T. C. Hsu, M. H. Hsieh, M. J. Jou, B. J. Lee, T.C. Lu, H.C. Kuo, and S.C. Wang, "Enhancing Output Power of GaN-based LEDs Grown on Chemical Wet Etching Patterned Sapphire Substrate," *IEEE Photonic Technology Letter, Vol. 18, pp.1152-1154, 2006* .

8. **Y. J. Lee,** H.C. Kuo, T.C. Lu, H.C. Kuo, B.J.Su, and S.C. Wang, "Fabrication and characterization of GaN-based LEDs grown on Chemical Wet Etching Patterned Sapphire Substrate," *Journal of The Electrochemical Society,* **153** (12) G1106-G1111,**2006** .

9. **Y. J. Lee**, T.C. Lu, H.C. Kuo, Member, IEEE, and S.C. Wang, Senior Member, IEEE, "Highly Light-Extraction GaN-based LEDs With Double Diffuse Surfaces," *IEEE Journal Of Quantum Electronics*, VOL. 42, NO. 12, pp.1196-1201**, 2006.**

10. T. S. Ko, T. C. Wang, R. C. Gao, **Y. J. Lee**, T. C. Lu, H. C. Kuo and S. C. Wang, "InGaN/GaN nanostripe grown on pattern sapphire by metal organic chemical vapor deposition," **Applied Physics Letters 90**, 013110 ,**2007** .

11. **Y. J. Lee**, H. C. Kuo, S. C. Wang, T. C. Hsu, M. H. Hsieh, M. J. Jou, and B. J.Lee "Nano-roughening n-side surface of AlGaInP-based LEDs for increasing extraction efficiency", *Material Science and Engineering: B,* Volume: 138, Issue: 2, March 25, pp. 157-160, **2007**

12. **Y. J. Lee**, T.C. Lu, H.C. Kuo and S.C. Wang, "High Brightness GaN-based Light Emitting Diodes," *IEEE Journal of Display Technology,* VOL. 3, NO. 2, pp.118-125**, 2007.**

13. **Y. J. Lee**, P.C. Lin, T.C. Lu, H.C. Kuo and S.C. Wang, "Dichromatic InGaN-based white light-emitting-diodes by using laser lift-off and wafer-bonding schemes," **Applied Physics Letters 90**, 161115 ,**2007**

14. **Ya-Ju Lee**, T.C. Lu, H.C. Kuo, S.C. Wang ,Kar Wai Ng, and Kei May Lau, Zu-Po Yang, Allan S.P. Chang, and Shawn-Yu Lin ,"Study of GaN-based light emitting diodes grown on chemical wet etching-patterned sapphire substrate with V-shaped pits roughening surfaces," **Journal of Applied Physics.** (Submitted).

Selected Presentation

1. **Y. J. Lee** , T.C. Lu, H.C. Kuo, S.C. Wang, M. J. Liou, C.W. Chang, T. C. Hsu, M. H. Hsieh, M. J. Jou, and B. J. Lee, "High brightness AlGaInP-based light emitting diodes by adopting the stripe-patterned omni-directional reflector, OPT, Taiwan *(台灣光電年會)*, 2005.

2. **Y. J. Lee**, T. C. Hsu, H.C. Kuo and S.C. Wang, "Improvement in light-output efficiency of Near-Ultraviolet InGaN–GaN LEDs Fabricated on Stripe Patterned Sapphire Substrates", International Quantum Electronics Conference 2005 and the Pacific Rim Conference on Lasers and Electro-Optics 2005 (IQEC/CLEO-PR 2005), Tokyo, Japan, July 2005.

3. **Y. J. Lee,** T.C. Lu, H.C. Kuo, S.C. Wang, T. C. Hsu, M. H. Hsieh, M. J. Jou, and B. J. Lee, "High Brightness AlGaInP-based LEDs with the StripePatterned Omni-Directional Reflector," IEEE/OSA Conference on Lasers and Electro-Optics 2006 (CLEO 2006), Pres. no.: CTuE3, Long Beach, California, United States, May 2006.

4. **Y. J. Lee**, T.C. Lu, H.C. Kuo, S.C. Wang, J.M.Hwang T. C. Hsu, M. H. Hsieh, M. J. Jou, and B. J. Lee, "Fabricating GaN-based LEDs with V-Shape Sapphire Facet Mirror by Double Transferred Scheme," IEEE/OSA Conference on Lasers and Electro-Optics 2006 (CLEO 2006), Pres. no.: CTuN3, Long Beach, California, United States, May 2006.

5. <u>李亞儒**(Y.J. Lee**）</u>, 徐大正(T.C.Hsu), 謝明勳(M.H.Hsieh), 周銘俊(M.J.Jou), 李秉傑（ B.J.Lee),盧廷昌（T.C. Lu）,郭浩中(H.C. Kuo）,王興宗（S.C. Wang）, "Fabrication and characterization of GaN-based LEDs grown on chemical wet-etched patterned sapphire substrate," 第八屆兩岸三地光電子學術研討會, Shan-Xi, China, June, 2006.

6. **Y. J. Lee**, H.C. Kuo **(Invited)**, T.C. Lu, S.C. Wang and C.F. Lin, "Improvement in the extraction efficiency of AlGaInP and GaN thin film LEDs via n-side surface roughening," The Electrochemical Society (ECS) Meeting, Cancun, Mexico, 2006.

7. **Y. J. Lee**, T.C. Lu, H.C. Kuo, S.C. Wang, T. C. Hsu, and M. H. Hsieh "Fabrication and characterization of GaN-based LEDs grown on chemical wet-etched patterned sapphire substrates (CWE-PSS)," International Workshop on Nitride (IWN 2006), Kyoto, Japan, Oct. 2006

8. **Y. J. Lee**, T.C. Lu, H.C. Kuo, and S.C. Wang, "High-Light-Extraction GaN-Based Vertical LEDs with Double Diffuse Surfaces," OPT, Taiwan *(台灣 光電年會)*, 2006.

9. **Y. J. Lee**, T.C. Lu, H.C. Kuo, and S.C. Wang," High-Light-Extraction GaN-Based Vertical LEDs with Double Diffuse Surfaces," IEEE/OSA Conference on Lasers and Electro-Optics 2007 (CLEO 2007), Pres. no.: CTuI4, Baltimore, Maryland, United States, May 2007.

10. **Y. J. Lee**, C. H. Chiu, T.C. Lu, H.C. Kuo, S.C. Wang ,K. W. Ng, K. M. Lau, Z. P. Yang, Allan S.P. Chang, and S. Y. Lin "Simultaneously enhancing internal and extraction efficiencies of GaN-based light emitting diodes via chemical-wet-etching patterned-sapphire-substrate, 212th The Electrochemical Society (ECS) Meeting , Washington, DC, Oct. 2007.
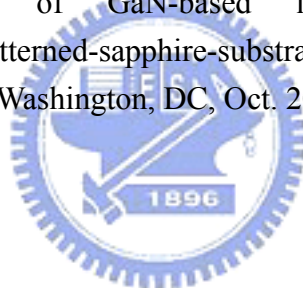
Curriculum Vitae

- **Name:** 李亞儒 (Ya-Ju Lee)
  Date of Birth: July 26th, 1978
  Birth Place: Kaohsiung, Taiwan

Academic Record:

- **Visiting Scholar (2007-2008)**
  Future Chip Constellation (FCC)
  Rensselaer Polytechnic Institute(壬色列理工學院),Troy, New York

- **Ph.D (2007)**
  Department of Photonics
  National Chiao Tung University (交通大學) ,Taiwan
  Thesis Title:
   **Research on Light Emission Enhancement of III-V Light- Emitting Diodes
   by Surface Modified Techniques**

- **M.S (2002)**
  Department of Photonic & Institute of Electro-Optical Engineering,
  National Chiao Tung University (交通大學), Taiwan
  Thesis Title:
   **The Study of 850 nm Oxidized and Implanted Vertical Cavity Surface
   Emitting Lasers (VCSELs)**

- **B.S (2000)**
  Department of Physics,
  National Central University (中央大學), Taiwan